https://doi.org/10.1016/j.compstruct.2020.112517

Free vibration and damage identification of cracked functionally graded plates

L. F. Zhu [a], L. L. Ke [a,b*], Y. Xiang [c] , X. Q. Zhu [d]

[a] *Department of Mechanics, Beijing Jiaotong University, Beijing, 100044, China*

[b] *School of Mechanical Engineering, Tianjin University, Tianjin, 300350, China*

[c] *School of Engineering, Western Sydney University, Penrith, NSW 2751, Australia*

[d] *School of Civil and Environmental Engineering, University of Technology Sydney, Broadway NSW 2007, Australia*

Abstract.

This paper investigates the free vibration and crack identification of functionally graded material (FGM) plates with a through-width edge crack. The material properties of the FGM plates change continuously with the power law distribution along the plate thickness direction. The crack in an FGM plate is simulated as a massless rotational spring and the plate is separated into two sub-plates at the crack location connected by the line spring. The stress intensity factor (SIF) in the FGM strip is calculated to determine the stiffness of the spring. The governing equations of cracked FGM plates are derived from the Mindlin plate theory and solved by the differential quadrature (DQ) method to obtain modal parameters. The vibrational mode of a cracked FGM plate is analyzed by utilizing continuous wavelet transform (CWT). A novel damage index (DI) is developed based on calculated wavelet coefficients to localize the crack in FGM plates. This method can localize the crack accurately and reduce the edge effect even with the measurement noise.

Keywords: Functionally graded plate; Damage index; Edge crack; Damage identification; Continuous wavelet transform

*Corresponding author. E-mail address: llke@bjtu.edu.cn (Liao-Liang Ke)

1. Introduction

To address the challenges in scientific and industrial applications, composite materials with continuous spatial change in constituents and material properties were produced to improve their thermo-mechanical performance as thermal barrier and are named as the functionally graded materials (FGMs) [1-3]. FGMs can be designed with desirable mechanical, physical and electrical properties so that they can be applied in many areas, such as automobile, defense, energy, biomedical, aerospace, etc. [4]. In these application areas, FGM plate-like structures such as rectangular, circular, annular, trapezoidal and skew plates are important components of industrial structures, e.g. the automotive turbocharger turbine [5], cutting-tool [6], wind tunnel blade [7], broadband ultrasonic transducers [8], B-pillar [9], etc. Since FGM plates are in general used in hard working environments, damages to the plates often occur. Therefore, it is vitally important to estimate the locations and severity of damages in FGM plate-like structures.

It is well-known that damages can reduce the local stiffness and change the vibration characteristics of structures. Base on the vibration characteristics, many frequency-based damage identification methods for structures were developed in the last three decades. Frequency-based methods were achieved by monitoring the natural frequency change of structures [10]. Pan et al. [11] experimentally detected the delamination in the composite curved plates based on surrogate assisted genetic algorithm and frequency shift polluted by noise. However, there are some limitations to predicate the damage location for frequency-based methods [12]. The database of frequency changes from different damage scenarios is needed to train the model for structural damage detection [13]. In general, the frequency change is insensitive to the structural local damage, and the uncertainties in numerical models, operational environments and measurement noise have a significant impact on the accuracy of structural damage identification.

Mode shape is another modal parameter which can be easily obtained and used to implement damage localization in structures. The mode of a structure can provide the local information of the structure comparing with the natural frequency of the structure. Moreover, with the development of the non-contact vibration measurement, the mode shape can be measured precisely and obtained by enough sampling points [14-16]. However, the mode shape is insensitive to damages [12]. In 1991, Pandey et al. [17] first proposed the modal curvature shapes change method to identify the presence of the crack and its location for damaged beams. For plate-like structures, Araújo dos Santos et al. [18] studied the damage detection in a carbon fiber reinforced epoxy plate by using the modal curvature differences. Actually, the

differentiation will enlarge the measurement errors in the modal shape for the method based on the curvature shape [19].

Note that the aforementioned methods require that the model parameters from intact structures are obtained as the baseline when comparing with the model parameters from damaged structures. In general, an imprecise baseline may result in the error of the change of model parameters between intact and damaged structures. Therefore, baseline-free damage detection methods are much suitable for practical applications. The baseline-free methods were proposed by many researchers, including gapped smoothing method, fractal dimension method, wavelet-based method etc. [20-22]. The wavelet-based methods were developed by using wavelet transform in which the static deflection [23], the mode shape [24], the operational deflection shapes [25] or the active thermography [26] can be treated as the input signal. By observing the sudden change in wavelet coefficients, the wavelet transform enables the singularity in the input signal to be detected [27]. In other words, damage location may be forecasted from the sudden change of wavelet coefficients at the spatial position. Douka et al. [28] employed one-dimensional continuous wavelet transform (CWT) method in the damage detection of plates with an all-over part-through crack. Fan and Qiao [29] took two-dimensional CWT of mode shapes to identify the crack location in plates. Katunin [30] presented numerical and experimental investigations for the damage identification based on two-dimensional discrete wavelet transform. This method was effective for localizing the damage in the plate with crack, notch and spatial damages. Zhou and Li [31] proposed a damage index for detecting sandwich composite plates with damaged core. Xu et al. [32] proposed a damage identification method for of plate-like structures by employing the mode shape curvatures under noisy conditions. The calculated wavelet coefficients were equal to the sum of wavelet coefficients produced from the CWT of mode shape curvatures along the length and width directions.

According to the aforementioned literatures, many modal based damage identification methods are studied in homogeneous and laminated structures. A little research has been reported on damage identification of FGM structures. Khiem and Huyen [33] presented frequency-based crack identification method for FGM beams. A crack identification method is developed by Yu and Chu [34] based on the natural frequency change between the intact and cracked FGM beams. Yang et al. [35] investigated the damage identification of FGM beams based on the change of the modal strain energy. Lu et al. [36] detected the damages in the axial FGM beam by employing model updating approach. For the vibration-based damage identification method of FGM plates, the model parameters need to be obtained

first for cracked FGM plates. Studies on the vibration analysis of cracked FGM plates have been reported in [37-42].

In this paper, the free vibration and crack identification of FGM plates with a through-width edge crack are presented. The material properties of FGM plates vary continuous in the plate thickness direction as the power law distribution. The crack is simulated as a massless line rotational spring. The stiffness of the line spring depends on the stress intensity factors (SIFs) which are determined from the material properties, the graded index and the crack depth. SIFs are calculated by using the ABAQUS software package. The governing equations of a cracked FGM plate are solved to obtain the eigen frequencies and the corresponding mode shapes. The mode shapes are decomposed into wavelet components by utilizing the CWT along the *x*- and *y*-directions, respectively. Based on calculated wavelet coefficients, a novel damage index (DI) is proposed to localize the crack in FGM plates under normal and noise conditions.

2. Linear rotational spring model

Fig. 1a depicts an FGM plate with a through-width edge crack of depth *a* located at $x = L_1$. The thickness, length and width of the plate are *h*, L_x and L_y, respectively. The Young's modulus $E(z)$, Poisson's ratio $\mu(z)$ and mass density $\rho(z)$ of FGM plates change with the power law function in the *z*-axis direction, i.e.

$$E(z) = \left(E_b - E_t\right)\left(\frac{z}{h} + \frac{1}{2}\right)^n + E_t, \tag{1}$$

$$\mu(z) = \left(\mu_b - \mu_t\right)\left(\frac{z}{h} + \frac{1}{2}\right)^n + \mu_t, \tag{2}$$

$$\rho(z) = \left(\rho_b - \rho_t\right)\left(\frac{z}{h} + \frac{1}{2}\right)^n + \rho_t, \tag{3}$$

where *n* is the gradient index and the subscripts *t* and *b* represent the top and bottom surfaces of FGM plates, respectively.

In Fig. 1b, the through-width edge crack is replaced by a massless rotational spring. The cracked FGM plate is composed of two sub-plates connected by a spring. In the rotational spring model, only the discontinuity of the bending slop at the crack section is considered. This model will be used to analyze the vibration of FGM plates. The relationship between bending stiffness S_T and the flexibility *F* of the

spring is defined by

$$S_T = \frac{1}{F}, \tag{4}$$

and the flexibility can be calculated from [43]

$$\frac{\left[1-\mu^2(a)\right]K_{\mathrm{I}}^2}{E(a)} = \frac{M_c^2}{2}\frac{\mathrm{d}F}{\mathrm{d}a}, \tag{5}$$

where K_{I} is the mode I SIF under the pure bending moment M_c; $E(a)$ and $\mu(a)$ are the Young's modulus and Poisson's ratio at the crack tip, respectively.

K_{I} is calculated from the J-contour integral within the software ABAQUS. Fig. 2 shows a multilayer model of FGM strip for the numerical calculation of SIFs. A couple of opposite pure bending moment M_c is applied to the ends of the edge-cracked layer with thickness h and the length L. The collapsed elements are used at the crack tip. The element type is CPS8R. To simulate the graded properties of FGM layer, the layer is discretized into N_f sub-layers. The thickness of the l-th sub-layer h_l is defined by

$$h_l = \begin{cases} \dfrac{a-0.01h}{30\chi}, & l = 1,2,...,30\chi, \\ 0.02h, & l = 1+30\chi, \\ \dfrac{h-a-0.01h}{30(1-\chi)}, & l = 2+30\chi,...,31, \end{cases} \tag{6}$$

where $\chi = a/h$ is the ratio of the crack depth and layer thickness and is chosen as 0.1, 0.2, …., 0.7 in this study.

The Young's modulus and Poisson's ratio of each sub-layer can be calculated by using the equivalent discrete layer approach [44]

$$E_l = \int_{z_b}^{z_u} \frac{E(z)}{h_l}\mathrm{d}z,\ \mu_l = \int_{z_b}^{z_u} \frac{\mu(z)}{h_l}\mathrm{d}z,\ l = 1,2,\mathrm{K}\ ,31, \tag{7}$$

where z_u and z_b are the coordinates of the upper and lower faces of the l-th sub-layer, respectively. Then, SIFs can be calculated by using the ABAQUS software package and normalized as

$$\bar{K}_{\mathrm{I}} = \frac{K_{\mathrm{I}}}{\sigma\sqrt{\pi a}},\quad \sigma = \frac{6M}{h^2}. \tag{8}$$

The FGM plates in this study are made of SUS304 and Si_3N_4 on the top and bottom surfaces, respectively. Table 1 gives material properties of SUS304 and Si_3N_4. Table 2 presents the SIFs with different grade index n and crack depth ratio χ. Based on the values of the mode I SIFs in Table 2, the relationship between K_{I} and χ can be given by the Lagrange interpolation method [45]:

$$K_{\mathrm{I}} = \frac{6M\sqrt{\pi h\chi}}{h^2}\Phi(\chi), \quad \chi = \frac{a}{h}, \tag{9}$$

where the crack depth ratio $0<\chi \le 0.7$ and $\Phi(\chi)$ is given as

$$\begin{aligned} n=0: \quad \Phi(\chi) &= 1.157 - 2.21963\chi + 15.7218\chi^2 - 56.6562\chi^3 \\ &\quad + 133.451\chi^4 - 163.042\chi^5 + 86.8056\chi^6, \end{aligned} \tag{10a}$$

$$\begin{aligned} n=0.5: \quad \Phi(\chi) &= 1.0122 - 2.27355\chi + 20.0475\chi^2 - 76.9708\chi^3 \\ &\quad + 174.736\chi^4 - 202.417\chi^5 + 101.111\chi^6, \end{aligned} \tag{10b}$$

$$\begin{aligned} n=1: \quad \Phi(\chi) &= 0.9366 - 0.5017\chi + 3.28803\chi^2 - 7.89792\chi^3 \\ &\quad + 32.2569\chi^4 - 58.2083\chi^5 + 44.0278\chi^6, \end{aligned} \tag{10c}$$

$$\begin{aligned} n=2: \quad \Phi(\chi) &= 0.9888 - 0.759933\chi + 3.04561\chi^2 - 4.41667\chi^3 \\ &\quad + 21.5694\chi^4 - 44.0\chi^5 + 36.9444\chi^6, \end{aligned} \tag{10d}$$

Substituting Eq. (9) into Eq. (5) yields

$$F = \int_0^{\chi} \frac{72\pi\left[1-\mu^2(a)\right]\chi\Phi^2(\chi)}{E(a)h^2}\mathrm{d}\chi. \tag{11}$$

Then, the bending stiffness of the rotational spring can be calculated from Eqs. (4) and (11).

3. Vibration of cracked FGM plates

According to the Mindlin hypothesis, the displacement field of an FGM plate can be given as

$$\hat{u}(x,y,z,t) = u(x,y,t) + z\phi_x(x,y,t), \tag{12}$$

$$\hat{v}(x,y,z,t) = v(x,y,t) + z\phi_y(x,y,t), \tag{13}$$

$$\hat{w}(x,y,z,t) = w(x,y,t), \tag{14}$$

where $u(x,y,t)$, $v(x,y,t)$ and $w(x,y,t)$ are the displacement of the point on the middle plane along the x-, y- and z-directions, respectively; $\phi_x(x,y,t)$ and $\phi_y(x,y,t)$ are the rotations of a transverse normal about y- and x-axis, respectively; t is the time.

The strains are given by

$$\varepsilon_{xx} = \frac{\partial u}{\partial x} + z\frac{\partial \phi_x}{\partial x}, \quad \varepsilon_{yy} = \frac{\partial v}{\partial y} + z\frac{\partial \phi_y}{\partial y}, \quad \varepsilon_{zz} = 0, \tag{15a}$$

$$\gamma_{xy} = \frac{\partial u}{\partial y} + \frac{\partial v}{\partial x} + z\left(\frac{\partial \phi_x}{\partial y} + \frac{\partial \phi_y}{\partial x}\right), \quad \gamma_{xz} = \phi_x + \frac{\partial w}{\partial x}, \quad \gamma_{yz} = \phi_y + \frac{\partial w}{\partial y}. \tag{15b}$$

The stresses are

$$\sigma_{xx} = Q_{11}\varepsilon_{xx} + Q_{12}\varepsilon_{yy}, \quad \sigma_{yy} = Q_{11}\varepsilon_{yy} + Q_{12}\varepsilon_{xx}, \tag{16a}$$

$$\tau_{xy} = Q_{66}\gamma_{xy}, \quad \tau_{xz} = Q_{66}\gamma_{xz}, \quad \tau_{yz} = Q_{66}\gamma_{yz}, \tag{16b}$$

where

$$Q_{11} = \frac{E(z)}{1-\mu^2(z)}, \quad Q_{12} = \frac{\mu(z)E(z)}{1-\mu^2(z)}, Q_{66} = \frac{E(z)}{2\left[1+\mu(z)\right]}. \tag{17}$$

The internal forces are

$$\left\{N_{xx}, N_{yy}, N_{xy}\right\} = \int_{-h/2}^{h/2}\left\{\sigma_{xx}, \sigma_{yy}, \tau_{xy}\right\}\, \mathrm{d}z, \tag{18a}$$

$$\left\{M_{xx}, M_{yy}, M_{xy}\right\} = \int_{-h/2}^{h/2}\left\{\sigma_{xx}, \sigma_{yy}, \tau_{xy}\right\} z\, \mathrm{d}z, \tag{18b}$$

$$\left\{Q_x, Q_y\right\} = \kappa\int_{-h/2}^{h/2}\left\{\tau_{xz}, \tau_{yz}\right\}\, \mathrm{d}z, \tag{18c}$$

where κ is the shear correction factor. According to Efraim and Eisenberger [46], the shear correction factor of FGM plates can be expressed as

$$\kappa = \frac{5}{6-\left(\mu_b V_b + \mu_t V_t\right)}, \tag{19}$$

where V_b and V_t denotes the volume fraction of each materials. The stiffness components are defined as

$$\left\{A_{11}, A_{12}, A_{66}\right\} = \int_{-h/2}^{h/2}\left\{Q_{11}, Q_{12}, Q_{66}\right\}\mathrm{d}z, \tag{20a}$$

$$\left\{B_{11}, B_{12}, B_{66}\right\} = \int_{-h/2}^{h/2}\left\{Q_{11}, Q_{12}, Q_{66}\right\} z\mathrm{d}z, \tag{20b}$$

$$\left\{D_{11}, D_{12}, D_{66}\right\} = \int_{-h/2}^{h/2}\left\{Q_{11}, Q_{12}, Q_{66}\right\} z^2\mathrm{d}z\,. \tag{20c}$$

The virtual strain energy δU of the cracked FGM plate is

$$
\begin{aligned}
\delta U = & \int_0^{L_y} K_T \left[\phi_{x1}\left(L_1,y\right)-\phi_{x2}\left(L_1,y\right)\right]\delta\left[\phi_{x1}\left(L_1,y\right)-\phi_{x2}\left(L_1,y\right)\right]\mathrm{d}y \\
& +\int_0^{L_1}\int_0^{L_y}\left[N_{xx1}\delta\frac{\partial u_1}{\partial x}+M_{xx1}\delta\frac{\partial \phi_{x1}}{\partial x}+Q_{x1}\delta\left(\phi_{x1}+\frac{\partial w_1}{\partial x}\right)+N_{xy1}\delta\left(\frac{\partial u_1}{\partial y}+\frac{\partial v_1}{\partial x}\right)\right. \\
& \left.+M_{xy1}\delta\left(\frac{\partial \phi_{x1}}{\partial y}+\frac{\partial \phi_{y1}}{\partial x}\right)+N_{yy1}\delta\frac{\partial v_1}{\partial y}+M_{yy1}\delta\frac{\partial \phi_y}{\partial y}+Q_{y1}\delta\left(\phi_{y1}+\frac{\partial w_1}{\partial y}\right)\right]\mathrm{d}y\mathrm{d}x \\
& +\int_{L_1}^{L_x}\int_0^{L_y}\left[N_{xx2}\delta\frac{\partial u_2}{\partial x}+M_{xx2}\delta\frac{\partial \phi_{x2}}{\partial x}+Q_{x2}\delta\left(\phi_{x2}+\frac{\partial w_2}{\partial x}\right)+N_{xy2}\delta\left(\frac{\partial u_2}{\partial y}+\frac{\partial v_2}{\partial x}\right)\right. \\
& \left.+M_{xy2}\delta\left(\frac{\partial \phi_{x2}}{\partial y}+\frac{\partial \phi_{y2}}{\partial x}\right)+N_{yy2}\delta\frac{\partial v_2}{\partial y}+M_{yy2}\delta\frac{\partial \phi_{y2}}{\partial y}+Q_{y2}\delta\left(\phi_{y2}+\frac{\partial w_2}{\partial y}\right)\right]\mathrm{d}y\mathrm{d}x.
\end{aligned}
\tag{21}
$$

The virtual kinetic energy is

$$
\begin{aligned}
\delta K = & \int_0^{L_1}\int_0^{L_y}\left[I_0\left(\frac{\partial u_1}{\partial t}\delta\frac{\partial u_1}{\partial t}+\frac{\partial v_1}{\partial t}\delta\frac{\partial v_1}{\partial t}+\frac{\partial w_1}{\partial t}\delta\frac{\partial w_1}{\partial t}\right)+I_1\left(\frac{\partial u_1}{\partial t}\delta\frac{\partial \phi_{x1}}{\partial t}+\frac{\partial \phi_{x1}}{\partial t}\delta\frac{\partial u_1}{\partial t}\right.\right. \\
& \left.\left.+\frac{\partial v_1}{\partial t}\delta\frac{\partial \phi_{y1}}{\partial t}+\frac{\partial \phi_{y1}}{\partial t}\delta\frac{\partial v_1}{\partial t}\right)+I_2\left(\frac{\partial \phi_{x1}}{\partial t}\delta\frac{\partial \phi_{x1}}{\partial t}+\frac{\partial \phi_{y1}}{\partial t}\delta\frac{\partial \phi_{y1}}{\partial t}\right)\right]\mathrm{d}y\mathrm{d}x \\
& +\int_{L_1}^{L_x}\int_0^{L_y}\left[I_0\left(\frac{\partial u_2}{\partial t}\delta\frac{\partial u_2}{\partial t}+\frac{\partial v_2}{\partial t}\delta\frac{\partial v_2}{\partial t}+\frac{\partial w_2}{\partial t}\delta\frac{\partial w_2}{\partial t}\right)+I_1\left(\frac{\partial u_2}{\partial t}\delta\frac{\partial \phi_{x2}}{\partial t}+\frac{\partial \phi_{x2}}{\partial t}\delta\frac{\partial u_2}{\partial t}\right.\right. \\
& \left.\left.+\frac{\partial v_2}{\partial t}\delta\frac{\partial \phi_{y2}}{\partial t}+\frac{\partial \phi_{y2}}{\partial t}\delta\frac{\partial v_2}{\partial t}\right)+I_2\left(\frac{\partial \phi_{x2}}{\partial t}\delta\frac{\partial \phi_{x2}}{\partial t}+\frac{\partial \phi_{y2}}{\partial t}\delta\frac{\partial \phi_{y2}}{\partial t}\right)\right]\mathrm{d}y\mathrm{d}x,
\end{aligned}
\tag{22}
$$

where the subscript 1, 2 denotes the left sub-plate and right sub-plate; I_0, I_1 and I_2 are inertia terms

$$
\left\{I_0,I_1,I_2\right\}=\int_{-h/2}^{h/2}\rho\left(z\right)\left\{1,z,z^2\right\}\mathrm{d}z. \tag{23}
$$

By using the Hamilton principle,

$$
\int_0^t\left(\delta U-\delta K\right)\mathrm{d}t=0, \tag{24}
$$

the governing equations of cracked FGM plates are derived as

$$
\delta u_i:\ \frac{\partial N_{xxi}}{\partial x_i}+\frac{\partial N_{xyi}}{\partial y_i}=I_0\frac{\partial^2 u_i}{\partial t^2}+I_1\frac{\partial^2 \phi_{xi}}{\partial t^2}, \tag{25}
$$

$$
\delta v_i:\ \frac{\partial N_{xyi}}{\partial x_i}+\frac{\partial N_{yyi}}{\partial y_i}=I_0\frac{\partial^2 v_i}{\partial t^2}+I_1\frac{\partial^2 \phi_{yi}}{\partial t^2}, \tag{26}
$$

$$
\delta w_i:\ \frac{\partial Q_{xi}}{\partial x_i}+\frac{\partial Q_{yi}}{\partial y_i}=I_0\frac{\partial^2 w_i}{\partial t^2}, \tag{27}
$$

$$
\delta \phi_{xi}:\ \frac{\partial M_{xxi}}{\partial x_i}+\frac{\partial M_{xyi}}{\partial y_i}-Q_{xi}=I_1\frac{\partial^2 u_i}{\partial t^2}+I_2\frac{\partial^2 \phi_{xi}}{\partial t^2}, \tag{28}
$$

$$\delta\phi_{yi}:\ \frac{\partial M_{xyi}}{\partial x_i}+\frac{\partial M_{yyi}}{\partial y_i}-Q_{yi}=I_1\frac{\partial^2 v_i}{\partial t^2}+I_2\frac{\partial^2\phi_{yi}}{\partial t^2}. \tag{29}$$

The boundary conditions satisfy

$$u_i=0 \text{ or } N_{xxi}=0,\ v_i=0 \text{ or } N_{xyi}=0,\ w_i=0 \text{ or } Q_{xi}=0, \tag{30a}$$

$$\phi_{xi}=0 \text{ or } M_{xxi}=0,\ \phi_{yi}=0 \text{ or } M_{xyi}=0, \tag{30b}$$

at $x_1=0$ and $x_2=L_x$, where i=1, 2;

$$u_i=0 \text{ or } N_{xyi}=0,\ v_i=0 \text{ or } N_{yyi}=0,\ w_i=0 \text{ or } Q_{yi}=0, \tag{31a}$$

$$\phi_{xi}=0 \text{ or } M_{xxi}=0,\ \phi_{yi}=0 \text{ or } M_{yyi}=0, \tag{31b}$$

at $y_i=0, L_y$, where i=1, 2.

Meanwhile, the compatibility conditions at $x=L_1$ require

$$u_1(L_1,y_1)=u_2(L_1,y_2),\quad v_1(L_1,y_1)=v_2(L_1,y_2),\quad w_1(L_1,y_1)=w_2(L_1,y_2), \tag{32a}$$

$$\phi_{y1}(L_1,y_1)=\phi_{y2}(L_1,y_2),\ N_{xx1}(L_1,y_1)=N_{xx2}(L_1,y_2),\ N_{xy1}(L_1,y_1)=N_{xy2}(L_1,y_2), \tag{32b}$$

$$M_{xx1}(L_1,y_1)=M_{xx2}(L_1,y_2),\quad M_{xy1}(L_1,y_1)=M_{xy2}(L_1,y_2),\ Q_{x1}(L_1,y_1)=Q_{x2}(L_1,y_2), \tag{32c}$$

$$S_T\left[\phi_{x1}(L_1,y_1)-\phi_{x2}(L_1,y_2)\right]=M_{xx1}\left(L_1,y_1\right). \tag{32d}$$

By introducing the dimensionless quantities

$$\zeta_1=\frac{x_1}{L_1},\quad \xi_1=\frac{y_1}{L_y},\ \alpha_1=\frac{L_1}{L_x},\quad \lambda_1=\frac{L_1}{L_y},\ \eta_1=\frac{L_1}{h}, \tag{33a}$$

$$\zeta_2=\frac{x_2}{L_x-L_1},\ \xi_2=\frac{y_2}{L_y},\ \alpha_2=\frac{L_x-L_1}{L_x},\quad \lambda_2=\frac{L_x-L_1}{L_y},\ \eta_2=\frac{L_x-L_1}{h}, \tag{33b}$$

$$\left(\bar{u}_i,\bar{v}_i,\bar{w}_i\right)=\frac{\left(u_i,v_i,w_i\right)}{h},\ \left(\bar{A}_{11},\bar{A}_{12},\bar{A}_{66}\right)=\frac{\left(A_{11},A_{12},A_{66}\right)}{A_c},\ \left(\bar{B}_{11},\bar{B}_{12},\bar{B}_{66}\right)=\frac{\left(B_{11},B_{12},B_{66}\right)}{A_c h}, \tag{33c}$$

$$\left(\bar{D}_{11},\bar{D}_{12},\bar{D}_{66}\right)=\frac{\left(D_{11},D_{12},D_{66}\right)}{A_c h^2},\ \Omega=\omega L_x\sqrt{\frac{I_c}{A_c}},\quad \tau=\frac{t}{L_x}\sqrt{\frac{A_c}{I_c}},\quad \bar{S}_T=\frac{S_T L_1}{A_c h^2}, \tag{33d}$$

where I_c and A_c are the value of I_0 and A_{11} of the homogeneous plate (n=0) i.e., $I_c=\rho_b h$ and $A_c=E_b h/\left(1-\mu_b{}^2\right)$.

Then, the governing equations can be rewritten as

$$\bar{A}_{11}\frac{\partial^2\bar{u}_i}{\partial\zeta_i^{\,2}}+\bar{B}_{11}\frac{\partial^2\bar{\phi}_{xi}}{\partial\zeta_i^{\,2}}+\lambda_i\left(\bar{A}_{12}+\bar{A}_{66}\right)\frac{\partial^2\bar{v}_i}{\partial\zeta_i\partial\xi_i}+\lambda_i\bar{B}_{66}\frac{\partial^2\bar{\phi}_{xi}}{\partial\zeta_i\partial\xi_i}+\lambda_i\bar{B}_{12}\frac{\partial^2\bar{\phi}_{yi}}{\partial\zeta_i\partial\xi_i}$$
$$+\lambda_i^{\,2}\bar{A}_{66}\frac{\partial^2\bar{u}_i}{\partial\xi_i^{\,2}}+\lambda_i^{\,2}\bar{B}_{33}\frac{\partial^2\bar{\phi}_{yi}}{\partial\xi_i^{\,2}}=\alpha_i^{\,2}\bar{I}_0\frac{\partial^2\bar{u}_i}{\partial\tau^2}+\alpha_i^{\,2}\bar{I}_1\frac{\partial^2\bar{\phi}_{xi}}{\partial\tau^2}, \tag{34}$$

$$\bar{A}_{66}\frac{\partial^2\bar{v}_i}{\partial\zeta_i^{\,2}}+\bar{B}_{66}\frac{\partial^2\bar{\phi}_{yi}}{\partial\zeta_i^{\,2}}+\lambda_i\left(\bar{A}_{12}+\bar{A}_{66}\right)\frac{\partial^2\bar{u}_i}{\partial\zeta_i\partial\xi_i}+\lambda_i\left(\bar{B}_{12}+\bar{B}_{66}\right)\frac{\partial^2\bar{\phi}_{xi}}{\partial\zeta_i\partial\xi_i}$$
$$+\lambda_i^{\,2}\bar{A}_{11}\frac{\partial^2\bar{v}_i}{\partial\xi_i^{\,2}}+\lambda_i^{\,2}\bar{B}_{11}\frac{\partial^2\bar{\phi}_{yi}}{\partial\xi_i^{\,2}}=\alpha_i^{\,2}\bar{I}_0\frac{\partial^2\bar{v}_i}{\partial\tau^2}+\alpha_i^{\,2}\bar{I}_1\frac{\partial^2\bar{\phi}_{yi}}{\partial\tau^2}, \tag{35}$$

$$\kappa\bar{A}_{66}\left[\frac{\partial^2\bar{w}_i}{\partial\zeta_i^{\,2}}+\eta_i\frac{\partial^2\bar{\phi}_{xi}}{\partial\zeta_i^{\,2}}+\lambda_i^{\,2}\bar{A}_{11}\frac{\partial^2\bar{w}_i}{\partial\xi_i^{\,2}}+\lambda_i\eta_i\frac{\partial^2\bar{\phi}_{yi}}{\partial\xi_i^{\,2}}\right]=\alpha_i^{\,2}\bar{I}_0\frac{\partial^2\bar{w}_i}{\partial\tau^2}, \tag{36}$$

$$\bar{B}_{11}\frac{\partial^2\bar{u}_i}{\partial\zeta_i^{\,2}}+\bar{D}_{11}\frac{\partial^2\bar{\phi}_{xi}}{\partial\zeta_i^{\,2}}+\lambda_i\left(\bar{B}_{12}+\bar{B}_{66}\right)\frac{\partial^2\bar{v}_i}{\partial\zeta_i\partial\xi_i}+\lambda_i\left(\bar{D}_{12}+\bar{D}_{66}\right)\frac{\partial^2\bar{\phi}_{yi}}{\partial\zeta_i\partial\xi_i}$$
$$+\lambda_i^{\,2}\bar{B}_{66}\frac{\partial^2\bar{u}_i}{\partial\xi_i^{\,2}}+\lambda_i^{\,2}\bar{D}_{33}\frac{\partial^2\bar{\phi}_{xi}}{\partial\xi_i^{\,2}}-\kappa\bar{A}_{66}\left(\eta_i^{\,2}\bar{\phi}_{xi}+\eta_i\frac{\partial\bar{w}_i}{\partial\zeta_i}\right)=\alpha_i^{\,2}\bar{I}_1\frac{\partial^2\bar{u}_i}{\partial\tau^2}+\alpha_i^{\,2}\bar{I}_2\frac{\partial^2\bar{\phi}_{xi}}{\partial\tau^2}, \tag{37}$$

$$\bar{B}_{66}\frac{\partial^2\bar{v}_i}{\partial\zeta_i^{\,2}}+\bar{D}_{66}\frac{\partial^2\bar{\phi}_{yi}}{\partial\zeta_i^{\,2}}+\lambda_i\left(\bar{B}_{12}+\bar{B}_{66}\right)\frac{\partial^2\bar{u}_i}{\partial\zeta_i\partial\xi_i}+\lambda_i\left(\bar{D}_{12}+\bar{D}_{66}\right)\frac{\partial^2\bar{\phi}_{xi}}{\partial\zeta_i\partial\xi_i}$$
$$+\lambda_i^{\,2}\bar{B}_{11}\frac{\partial^2\bar{v}_i}{\partial\xi_i^{\,2}}+\lambda_i^{\,2}\bar{D}_{11}\frac{\partial^2\bar{\phi}_{yi}}{\partial\xi_i^{\,2}}-\kappa\bar{A}_{66}\left(\eta_i^{\,2}\bar{\phi}_{yi}+\eta_i\lambda_i\frac{\partial\bar{w}_i}{\partial\zeta_i}\right)=\alpha_i^{\,2}\bar{I}_1\frac{\partial^2\bar{v}_i}{\partial\tau^2}+\alpha_i^{\,2}\bar{I}_2\frac{\partial^2\bar{\phi}_{yi}}{\partial\tau^2}. \tag{38}$$

The boundary conditions can be expressed in dimensionless form as

$$\bar{u}_i=\bar{v}_i=\bar{w}_i=\bar{\phi}_{xi}=\bar{\phi}_{yi}=0, \tag{39}$$

at $\zeta_1=0$ and $\zeta_2=1$, where *i*=1, 2;

$$\bar{u}_i=\bar{v}_i=\bar{w}_i=\bar{\phi}_{xi}=\bar{\phi}_{yi}=0, \tag{40}$$

at $\xi_i=0,1$, where *i*=1, 2, for the cracked FGM plate with all boundaries clamped (CCCC);

$$\bar{u}_i=\bar{v}_i=\bar{w}_i=\bar{\phi}_{yi}=0,\quad \bar{B}_{11}\frac{\partial\bar{u}_i}{\partial\zeta_i}+\bar{D}_{11}\frac{\partial\bar{\phi}_{xi}}{\partial\zeta_i}+\lambda_i\bar{B}_{12}\frac{\partial\bar{v}_i}{\partial\xi_i}+\lambda_i\bar{D}_{12}\frac{\partial\bar{\phi}_{yi}}{\partial\xi_i}=0, \tag{41}$$

at $\zeta_1=0$ and $\zeta_2=1$, where *i*=1, 2;

$$\bar{u}_i=\bar{v}_i=\bar{w}_i=\bar{\phi}_{xi}=0,\quad \bar{B}_{12}\frac{\partial\bar{u}_i}{\partial\zeta_i}+\bar{D}_{12}\frac{\partial\bar{\phi}_{xi}}{\partial\zeta_i}+\lambda_i\bar{B}_{11}\frac{\partial\bar{v}_i}{\partial\xi_i}+\lambda_i\bar{D}_{11}\frac{\partial\bar{\phi}_{yi}}{\partial\xi_i}=0, \tag{42}$$

at $\xi_i=0,1$, where *i*=1, 2, for the cracked FGM plate with all boundaries hinged (HHHH);

$$\bar{u}_1=\bar{v}_1=\bar{w}_1=\bar{\phi}_{x1}=\bar{\phi}_{y1}=0, \tag{43}$$

at $\zeta_1 = 0$;

$$\bar{A}_{11}\frac{\partial \bar{u}_2}{\partial \zeta_2} + \bar{B}_{11}\frac{\partial \bar{\phi}_{x2}}{\partial \zeta_2} + \lambda_2 \bar{A}_{12}\frac{\partial \bar{v}_2}{\partial \xi_2} + \lambda_2 \bar{B}_{12}\frac{\partial \bar{\phi}_{y2}}{\partial \xi_2} = 0, \tag{44a}$$

$$\bar{B}_{11}\frac{\partial \bar{u}_2}{\partial \zeta_2} + \bar{D}_{11}\frac{\partial \bar{\phi}_{x2}}{\partial \zeta_2} + \lambda_2 \bar{B}_{12}\frac{\partial \bar{v}_2}{\partial \xi_2} + \lambda_2 \bar{D}_{12}\frac{\partial \bar{\phi}_{y2}}{\partial \xi_2} = 0, \tag{44b}$$

$$\bar{A}_{66}\frac{\partial \bar{v}_2}{\partial \zeta_2} + \bar{B}_{66}\frac{\partial \bar{\phi}_{y2}}{\partial \zeta_2} + \lambda_2 \bar{A}_{66}\frac{\partial \bar{u}_2}{\partial \xi_2} + \lambda_2 \bar{B}_{66}\frac{\partial \bar{\phi}_{x2}}{\partial \xi_2} = 0, \tag{44c}$$

$$\bar{B}_{66}\frac{\partial \bar{v}_2}{\partial \zeta_2} + \bar{D}_{66}\frac{\partial \bar{\phi}_{y2}}{\partial \zeta_2} + \lambda_2 \bar{B}_{66}\frac{\partial \bar{u}_2}{\partial \xi_2} + \lambda_2 \bar{D}_{66}\frac{\partial \bar{\phi}_{x2}}{\partial \xi_2} = 0, \tag{44d}$$

$$\kappa \bar{A}_{66}\left(\eta_2 \bar{\phi}_{x2} + \frac{\partial \bar{w}_2}{\partial \zeta_2}\right) = 0, \tag{44e}$$

at $\zeta_2 = 1$;

$$\bar{A}_{12}\frac{\partial \bar{u}_i}{\partial \zeta_i} + \bar{B}_{12}\frac{\partial \bar{\phi}_{xi}}{\partial \zeta_i} + \lambda_i \bar{A}_{11}\frac{\partial \bar{v}_i}{\partial \xi_i} + \lambda_i \bar{B}_{11}\frac{\partial \bar{\phi}_{yi}}{\partial \xi_i} = 0, \tag{45a}$$

$$\bar{B}_{12}\frac{\partial \bar{u}_i}{\partial \zeta_i} + \bar{D}_{12}\frac{\partial \bar{\phi}_{xi}}{\partial \zeta_i} + \lambda_i \bar{B}_{11}\frac{\partial \bar{v}_i}{\partial \xi_i} + \lambda_i \bar{D}_{11}\frac{\partial \bar{\phi}_{yi}}{\partial \xi_i} = 0, \tag{45b}$$

$$\bar{A}_{66}\frac{\partial \bar{v}_i}{\partial \zeta_i} + \bar{B}_{66}\frac{\partial \bar{\phi}_{yi}}{\partial \zeta_i} + \lambda_i \bar{A}_{66}\frac{\partial \bar{u}_i}{\partial \xi_i} + \lambda_i \bar{B}_{66}\frac{\partial \bar{\phi}_{xi}}{\partial \xi_i} = 0, \tag{45c}$$

$$\bar{B}_{66}\frac{\partial \bar{v}_i}{\partial \zeta_i} + \bar{D}_{66}\frac{\partial \bar{\phi}_{yi}}{\partial \zeta_i} + \lambda_i \bar{B}_{66}\frac{\partial \bar{u}_i}{\partial \xi_i} + \lambda_i \bar{D}_{66}\frac{\partial \bar{\phi}_{xi}}{\partial \xi_i} = 0, \tag{45d}$$

$$\kappa \bar{A}_{66}\left(\eta_i \bar{\phi}_{yi} + \lambda_i \frac{\partial \bar{w}_i}{\partial \xi_i}\right) = 0, \tag{45e}$$

at $\xi_i = 0,1$, where *i*=1, 2, for the cantilever cracked FGM plate (CFFF).

The compatibility conditions at $\zeta_1 = 1$ or $\zeta_2 = 0$, can be rewritten in dimensionless form as

$$\bar{u}_1(1,\xi_1) = \bar{u}_2(0,\xi_2), \quad \bar{v}_1(1,\xi_1) = \bar{v}_2(0,\xi_2), \tag{46a}$$

$$\bar{w}_1(1,\xi_1) = \bar{w}_2(0,\xi_2), \ \bar{\phi}_{y1}(1,\xi_1) = \bar{\phi}_{y2}(0,\xi_2), \tag{46b}$$

$$\bar{S}_T\left[\phi_{x1}(1,\xi_1) - \phi_{x2}(0,\xi_2)\right] = \bar{B}_{11}\frac{\partial \bar{u}_1}{\partial \zeta_1} + \bar{D}_{11}\frac{\partial \bar{\phi}_{x1}}{\partial \zeta_1} + \lambda_1 \bar{B}_{12}\frac{\partial \bar{v}_1}{\partial \xi_1} + \lambda_1 \bar{D}_{12}\frac{\partial \bar{\phi}_{y1}}{\partial \xi_1} \tag{46c}$$

$$\begin{aligned}&\bar{A}_{11}\frac{\partial\bar{u}_1}{\partial\zeta_1}+\bar{B}_{11}\frac{\partial\bar{\phi}_{x1}}{\partial\zeta_1}+\lambda_1\bar{A}_{12}\frac{\partial\bar{v}_1}{\partial\xi_1}+\lambda_1\bar{B}_{12}\frac{\partial\bar{\phi}_{y1}}{\partial\xi_1}\\&=\frac{\alpha_1}{\alpha_2}\bar{A}_{11}\frac{\partial\bar{u}_2}{\partial\zeta_2}+\frac{\alpha_1}{\alpha_2}\bar{B}_{11}\frac{\partial\bar{\phi}_{x2}}{\partial\zeta_2}+\lambda_1\bar{A}_{12}\frac{\partial\bar{v}_2}{\partial\xi_2}+\lambda_1\bar{B}_{12}\frac{\partial\bar{\phi}_{y2}}{\partial\xi_2},\end{aligned}\tag{46d}$$

$$\begin{aligned}&\bar{B}_{11}\frac{\partial\bar{u}_1}{\partial\zeta_1}+\bar{D}_{11}\frac{\partial\bar{\phi}_{x1}}{\partial\zeta_1}+\lambda_1\bar{B}_{12}\frac{\partial\bar{v}_1}{\partial\xi_1}+\lambda_1\bar{D}_{12}\frac{\partial\bar{\phi}_{y1}}{\partial\xi_1}\\&=\frac{\alpha_1}{\alpha_2}\bar{B}_{11}\frac{\partial\bar{u}_2}{\partial\zeta_2}+\frac{\alpha_1}{\alpha_2}\bar{D}_{11}\frac{\partial\bar{\phi}_{x2}}{\partial\zeta_2}+\lambda_1\bar{B}_{12}\frac{\partial\bar{v}_2}{\partial\xi_2}+\lambda_1\bar{D}_{12}\frac{\partial\bar{\phi}_{y2}}{\partial\xi_2},\end{aligned}\tag{46e}$$

$$\begin{aligned}&\bar{A}_{66}\frac{\partial\bar{v}_1}{\partial\zeta_1}+\bar{B}_{66}\frac{\partial\bar{\phi}_{y1}}{\partial\zeta_1}+\lambda_1\bar{A}_{66}\frac{\partial\bar{u}_1}{\partial\xi_1}+\lambda_1\bar{B}_{66}\frac{\partial\bar{\phi}_{x1}}{\partial\xi_1}\\&=\frac{\alpha_1}{\alpha_2}\bar{A}_{66}\frac{\partial\bar{v}_2}{\partial\zeta_2}+\frac{\alpha_1}{\alpha_2}\bar{B}_{66}\frac{\partial\bar{\phi}_{y2}}{\partial\zeta_2}+\lambda_1\bar{A}_{66}\frac{\partial\bar{u}_2}{\partial\xi_2}+\lambda_1\bar{B}_{66}\frac{\partial\bar{\phi}_{x2}}{\partial\xi_2},\end{aligned}\tag{46f}$$

$$\begin{aligned}&\bar{B}_{66}\frac{\partial\bar{v}_1}{\partial\zeta_1}+\bar{D}_{66}\frac{\partial\bar{\phi}_{y1}}{\partial\zeta_1}+\lambda_1\bar{B}_{66}\frac{\partial\bar{u}_1}{\partial\xi_1}+\lambda_1\bar{D}_{66}\frac{\partial\bar{\phi}_{x1}}{\partial\xi_1}\\&=\frac{\alpha_1}{\alpha_2}\bar{B}_{66}\frac{\partial\bar{v}_2}{\partial\zeta_2}+\frac{\alpha_1}{\alpha_2}\bar{D}_{66}\frac{\partial\bar{\phi}_{y2}}{\partial\zeta_2}+\lambda_1\bar{B}_{66}\frac{\partial\bar{u}_2}{\partial\xi_2}+\lambda_1\bar{D}_{66}\frac{\partial\bar{\phi}_{x2}}{\partial\xi_2},\end{aligned}\tag{46g}$$

$$\eta_1\bar{\phi}_{x1}+\frac{\partial\bar{w}_1}{\partial\zeta_1}=\eta_1\bar{\phi}_{x2}+\frac{\alpha_1}{\alpha_2}\frac{\partial\bar{w}_2}{\partial\zeta_2}.\tag{46h}$$

4. Methodology

The differential quadrature (DQ) method is able to find approximate solutions of partial differential equations [47]. The displacement and their r_1-th and r_2-th partial derivatives, respectively, can be denoted in discretized domain as

$$\begin{aligned}&\left\{\bar{u}_i,\bar{v}_i,\bar{w}_i,\bar{\phi}_{xi},\bar{\phi}_{yi}\right\}=\\&\sum_{n=1}^{N}\sum_{m=1}^{M}l_n\left(\zeta_i\right)l_m\left(\xi_i\right)\left\{\bar{u}_{i,nm}\left(\zeta_{i,n},\xi_{i,m},\tau\right),\bar{v}_{i,nm}\left(\zeta_{i,n},\xi_{i,m},\tau\right),\bar{w}_{i,nm}\left(\zeta_{i,n},\xi_{i,m},\tau\right),\right.\\&\left.\bar{\phi}_{xi,nm}\left(\zeta_{i,n},\xi_{i,m},\tau\right),\bar{\phi}_{yi,nm}\left(\zeta_{i,n},\xi_{i,m},\tau\right)\right\}\end{aligned}\tag{47}$$

$$\begin{aligned}&\frac{\partial^{r_1}}{\partial\zeta_i^{\,r_1}}\frac{\partial^{r_2}}{\partial\zeta_i^{\,r_2}}\left\{\bar{u}_i,\bar{v}_i,\bar{w}_i,\bar{\phi}_{xi},\bar{\phi}_{yi}\right\}\Big|_{\zeta_i=\zeta_{i,k_1},\xi_i=\xi_{i,k_2}}=\\&\sum_{n=1}^{N}\sum_{m=1}^{M}C_{k_1n}^{(r_1)}C_{k_2m}^{(r_2)}\left\{\bar{u}_{i,nm}\left(\zeta_{i,n},\xi_{i,m},\tau\right),\bar{v}_{i,nm}\left(\zeta_{i,n},\xi_{i,m},\tau\right),\bar{w}_{i,nm}\left(\zeta_{i,n},\xi_{i,m},\tau\right),\right.\\&\left.\bar{\phi}_{xi,nm}\left(\zeta_{i,n},\xi_{i,m},\tau\right),\bar{\phi}_{yi,nm}\left(\zeta_{i,n},\xi_{i,m},\tau\right)\right\},\end{aligned}\tag{48}$$

where N and M are the total node numbers along the ζ_i and ξ_i axes, respectively; $l_n\left(\zeta_i\right)$ and

$l_m\left(\xi_i\right)$ are the Lagrange interpolation polynomials; $C_{nk_1}^{(r_1)}$ and $C_{mk_2}^{(r_2)}$ are weighting coefficients which are calculated by the recursive functions as shown in Ref. [47]. In the discretized domain, grid points are placed based on the Chebyshev–Gauss–Lobatto distribution, i.e.,

$$\zeta_{i,k_1}=\frac{1}{2}\left[1-\cos\left(\frac{\pi\left(k_1-1\right)}{N-1}\right)\right],k_1=1,2,\mathrm{K}\ ,N, \tag{49}$$

$$\xi_{i,k_2}=\frac{1}{2}\left[1-\cos\left(\frac{\pi\left(k_2-1\right)}{M-1}\right)\right],k_2=1,2,\mathrm{K}\ ,M. \tag{50}$$

The discretized governing equations are given as

$$\begin{aligned}
&\overline{A}_{11}\sum_{n=1}^{N}C_{k_1n}^{(2)}\overline{u}_{i,nk_2}+\overline{B}_{11}\sum_{n=1}^{N}C_{k_1n}^{(2)}\overline{\phi}_{xi,nk_2}+\lambda_i\left(\overline{A}_{12}+\overline{A}_{66}\right)\sum_{n=1}^{N}\sum_{m=1}^{M}C_{k_1n}^{(1)}C_{k_2m}^{(1)}\overline{v}_{i,nm}\\
&+\lambda_i\overline{B}_{66}\sum_{n=1}^{N}\sum_{m=1}^{M}C_{k_1n}^{(1)}C_{k_2m}^{(1)}\overline{\phi}_{xi,nm}+\lambda_i\overline{B}_{12}\sum_{n=1}^{N}\sum_{m=1}^{M}C_{k_1n}^{(1)}C_{k_2m}^{(1)}\overline{\phi}_{yi,nm}\\
&+\lambda_i^{\,2}\overline{A}_{66}\sum_{m=1}^{M}C_{k_2m}^{(2)}\overline{u}_{i,k_1m}+\lambda_i^{\,2}\overline{B}_{33}\sum_{m=1}^{M}C_{k_2m}^{(2)}\overline{\phi}_{yi,k_1m}=\alpha_i^{\,2}\overline{I}_0\ddot{\overline{u}}_i+\alpha_i^{\,2}\overline{I}_1\ddot{\overline{\phi}}_{xi},
\end{aligned} \tag{51}$$

$$\begin{aligned}
&\overline{A}_{66}\sum_{n=1}^{N}C_{k_1n}^{(2)}\overline{v}_{i,nk_2}+\overline{B}_{66}\sum_{n=1}^{N}C_{k_1n}^{(2)}\overline{\phi}_{yi,nk_2}+\lambda_i\left(\overline{B}_{12}+\overline{B}_{66}\right)\sum_{n=1}^{N}\sum_{m=1}^{M}C_{k_1n}^{(1)}C_{k_2m}^{(1)}\overline{\phi}_{xi,nm}\\
&+\lambda_i\left(\overline{A}_{12}+\overline{A}_{66}\right)\sum_{n=1}^{N}\sum_{m=1}^{M}C_{k_1n}^{(1)}C_{k_2m}^{(1)}\overline{u}_{i,nm}+\lambda_i^{\,2}\overline{A}_{11}\sum_{m=1}^{M}C_{k_2m}^{(2)}\overline{v}_{i,k_1m}\\
&+\lambda_i^{\,2}\overline{B}_{11}\sum_{m=1}^{M}C_{k_2m}^{(2)}\overline{\phi}_{yi,k_1m}=\alpha_i^{\,2}\overline{I}_0\ddot{\overline{v}}_i+\alpha_i^{\,2}\overline{I}_1\ddot{\overline{\phi}}_{yi},
\end{aligned} \tag{52}$$

$$\begin{aligned}
&\kappa\overline{A}_{66}\left[\sum_{n=1}^{N}C_{k_1n}^{(2)}\overline{w}_{i,nk_2}+\eta_i\sum_{n=1}^{N}C_{k_1n}^{(2)}\overline{\phi}_{xi,nk_2}\right.\\
&\left.+\lambda_i^{\,2}\overline{A}_{11}\sum_{m=1}^{M}C_{k_2m}^{(2)}\overline{w}_{i,k_1m}+\lambda_i\eta_i\sum_{m=1}^{M}C_{k_2m}^{(2)}\overline{\phi}_{yi,k_1m}\right]=\alpha_i^{\,2}\overline{I}_0\ddot{\overline{w}}_i,
\end{aligned} \tag{53}$$

$$\begin{aligned}
&\overline{B}_{11}\sum_{n=1}^{N}C_{k_1n}^{(2)}\overline{u}_{i,nk_2}+\overline{D}_{11}\sum_{n=1}^{N}C_{k_1n}^{(2)}\overline{\phi}_{xi,nk_2}+\lambda_i\left(\overline{B}_{12}+\overline{B}_{66}\right)\sum_{n=1}^{N}\sum_{m=1}^{M}C_{k_1n}^{(1)}C_{k_2m}^{(1)}\overline{v}_{i,nm}\\
&+\lambda_i\left(\overline{D}_{12}+\overline{D}_{66}\right)\sum_{n=1}^{N}\sum_{m=1}^{M}C_{k_1n}^{(1)}C_{k_2m}^{(1)}\overline{\phi}_{yi,nm}+\lambda_i^{\,2}\overline{B}_{66}\sum_{m=1}^{M}C_{k_2m}^{(2)}\overline{u}_{i,k_1m}+\lambda_i^{\,2}\overline{D}_{33}\sum_{m=1}^{M}C_{k_2m}^{(2)}\overline{\phi}_{yi,k_1m}\\
&-\kappa\overline{A}_{66}\left(\eta_i^{\,2}\overline{\phi}_{xi,k_1k_2}+\eta_i\sum_{n=1}^{N}C_{k_1n}^{(1)}\overline{w}_{i,nk_2}\right)=\alpha_i^{\,2}\overline{I}_1\ddot{\overline{u}}_i+\alpha_i^{\,2}\overline{I}_2\ddot{\overline{\phi}}_{xi},
\end{aligned} \tag{54}$$

$$\begin{aligned}
&\overline{B}_{66}\sum_{n=1}^{N}C_{k_1n}^{(2)}\overline{v}_{i,nk_2}+\overline{D}_{66}\sum_{n=1}^{N}C_{k_1n}^{(2)}\overline{\phi}_{yi,nk_2}+\lambda_i\left(\overline{B}_{12}+\overline{B}_{66}\right)\sum_{n=1}^{N}\sum_{m=1}^{M}C_{k_1n}^{(1)}C_{k_2m}^{(1)}\overline{u}_{i,nm}\\
&+\lambda_i\left(\overline{D}_{12}+\overline{D}_{66}\right)\sum_{n=1}^{N}\sum_{m=1}^{M}C_{k_1n}^{(1)}C_{k_2m}^{(1)}\overline{\phi}_{xi,nm}+\lambda_i^{\,2}\overline{B}_{11}\sum_{m=1}^{M}C_{k_2m}^{(2)}\overline{v}_{i,k_1m}+\lambda_i^{\,2}\overline{D}_{11}\sum_{m=1}^{M}C_{k_2m}^{(2)}\overline{\phi}_{yi,k_1m}\\
&-\kappa\overline{A}_{66}\left(\eta_i^{\,2}\overline{\phi}_{yi,k_1k_2}+\eta_i\lambda_i\sum_{m=1}^{M}C_{k_2m}^{(1)}\overline{w}_{i,k_1m}\right)=\alpha_i^{\,2}\overline{I}_1\ddot{\overline{v}}_i+\alpha_i^{\,2}\overline{I}_2\ddot{\overline{\phi}}_{yi},
\end{aligned} \tag{55}$$

where the second partial derivative about the dimensionless time τ is represent by the two over dots. The boundary conditions are discretized as follows:

$$\overline{u}_{i,k_1k_2} = \overline{v}_{i,k_1k_2} = \overline{w}_{i,k_1k_2} = \overline{\phi}_{xi,k_1k_2} = \overline{\phi}_{yi,k_1k_2} = 0, \tag{56}$$

at $\zeta_1 = 0$ and $\zeta_2 = 1$, where k_1 is equal to 1 and N when $\zeta_1 = 0$ and $\zeta_2 = 1$, respectively;

$$\overline{u}_{i,k_1k_2} = \overline{v}_{i,k_1k_2} = \overline{w}_{i,k_1k_2} = \overline{\phi}_{xi,k_1k_2} = \overline{\phi}_{yi,k_1k_2} = 0, \tag{57}$$

at $\xi_i = 0,1$, where k_2 is equal to 1 and M when $\xi_i = 0$ and $\xi_i = 1$, respectively, for CCCC cracked FGM plate;

$$\overline{B}_{11}\sum_{n=1}^{N} C_{k_1n}^{(1)}\overline{u}_{i,nk_2} + \overline{D}_{11}\sum_{n=1}^{N} C_{k_1n}^{(1)}\overline{\phi}_{xi,nk_2} + \lambda_i\overline{B}_{12}\sum_{m=1}^{M} C_{k_2m}^{(1)}\overline{v}_{i,k_1m} + \lambda_i\overline{D}_{12}\sum_{m=1}^{M} C_{k_2m}^{(1)}\overline{\phi}_{yi,k_1m} = 0 \tag{58a}$$

$$\overline{u}_{i,k_1k_2} = \overline{v}_{i,k_1k_2} = \overline{w}_{i,k_1k_2} = \overline{\phi}_{yi,k_1k_2} = 0, \tag{58b}$$

at $\zeta_1 = 0$ and $\zeta_2 = 1$, where k_1 is equal to 1 and N when $\zeta_1 = 0$ and $\zeta_2 = 1$, respectively;

$$\overline{B}_{12}\sum_{n=1}^{N} C_{k_1n}^{(1)}\overline{u}_{i,nk_2} + \overline{D}_{12}\sum_{n=1}^{N} C_{k_1n}^{(1)}\overline{\phi}_{xi,nk_2} + \lambda_i\overline{B}_{11}\sum_{m=1}^{M} C_{k_2m}^{(1)}\overline{v}_{i,k_1m} + \lambda_i\overline{D}_{11}\sum_{m=1}^{M} C_{k_2m}^{(1)}\overline{\phi}_{yi,k_1m} = 0 \tag{59a}$$

$$\overline{u}_{i,k_1k_2} = \overline{v}_{i,k_1k_2} = \overline{w}_{i,k_1k_2} = \overline{\phi}_{xi,k_1k_2} = 0, \tag{59b}$$

at $\xi_i = 0,1$, where k_2 is equal to 1 and M when $\xi_i = 0$ and $\xi_i = 1$, respectively, for HHHH cracked FGM plate;

$$\overline{u}_{1,1k_2} = \overline{v}_{1,1k_2} = \overline{w}_{1,1k_2} = \overline{\phi}_{x1,1k_2} = \overline{\phi}_{y1,1k_2} = 0, \tag{60}$$

at $\zeta_1 = 0$;

$$\overline{A}_{11}\sum_{n=1}^{N} C_{Nn}^{(1)}\overline{u}_{2,nk_2} + \overline{B}_{11}\sum_{n=1}^{N} C_{Nn}^{(1)}\overline{\phi}_{x2,nk_2} + \lambda_2\overline{A}_{12}\sum_{m=1}^{M} C_{k_2m}^{(1)}\overline{v}_{2,Nm} + \lambda_2\overline{B}_{12}\sum_{m=1}^{M} C_{k_2m}^{(1)}\overline{\phi}_{y2,Nm} = 0, \tag{61a}$$

$$\overline{B}_{11}\sum_{n=1}^{N} C_{Nn}^{(1)}\overline{u}_{2,nk_2} + \overline{D}_{11}\sum_{n=1}^{N} C_{Nn}^{(1)}\overline{\phi}_{x2,nk_2} + \lambda_2\overline{B}_{12}\sum_{m=1}^{M} C_{k_2m}^{(1)}\overline{v}_{2,Nm} + \lambda_2\overline{D}_{12}\sum_{m=1}^{M} C_{k_2m}^{(1)}\overline{\phi}_{y2,Nm} = 0, \tag{61b}$$

$$\overline{A}_{66}\sum_{n=1}^{N} C_{Nn}^{(1)}\overline{v}_{2,nk_2} + \overline{B}_{66}\sum_{n=1}^{N} C_{Nn}^{(1)}\overline{\phi}_{y2,nk_2} + \lambda_2\overline{A}_{66}\sum_{m=1}^{M} C_{k_2m}^{(1)}\overline{u}_{2,Nm} + \lambda_2\overline{B}_{66}\sum_{m=1}^{M} C_{k_2m}^{(1)}\overline{\phi}_{x2,Nm} = 0, \tag{61c}$$

$$\overline{B}_{66}\sum_{n=1}^{N} C_{Nn}^{(1)}\overline{v}_{2,nk_2} + \overline{D}_{66}\sum_{n=1}^{N} C_{Nn}^{(1)}\overline{\phi}_{y2,nk_2} + \lambda_2\overline{B}_{66}\sum_{m=1}^{M} C_{k_2m}^{(1)}\overline{u}_{2,Nm} + \lambda_2\overline{D}_{66}\sum_{m=1}^{M} C_{k_2m}^{(1)}\overline{\phi}_{x2,Nm} = 0, \tag{61d}$$

$$\kappa \bar{A}_{66}\left(\eta_2 \bar{\phi}_{x2,Nk_2}+\sum_{n=1}^{N} C_{Nn}^{(1)} \bar{w}_{2,nk_2}\right)=0, \tag{61e}$$

at $\zeta_2=1$;

$$\bar{A}_{12}\sum_{n=1}^{N} C_{k_1n}^{(1)} \bar{u}_{i,nk_2}+\bar{B}_{12}\sum_{n=1}^{N} C_{k_1n}^{(1)} \bar{\phi}_{xi,nk_2}+\lambda_i \bar{A}_{11}\sum_{m=1}^{M} C_{k_2m}^{(1)} \bar{v}_{i,k_1m}+\lambda_i \bar{B}_{11}\sum_{m=1}^{M} C_{k_2m}^{(1)} \bar{\phi}_{yi,k_1m}=0, \tag{62a}$$

$$\bar{B}_{12}\sum_{n=1}^{N} C_{k_1n}^{(1)} \bar{u}_{i,nk_2}+\bar{D}_{12}\sum_{n=1}^{N} C_{k_1n}^{(1)} \bar{\phi}_{xi,nk_2}+\lambda_i \bar{B}_{11}\sum_{m=1}^{M} C_{k_2m}^{(1)} \bar{v}_{i,k_1m}+\lambda_i \bar{D}_{11}\sum_{m=1}^{M} C_{k_2m}^{(1)} \bar{\phi}_{yi,k_1m}=0, \tag{62b}$$

$$\bar{A}_{66}\sum_{n=1}^{N} C_{k_1n}^{(1)} \bar{v}_{i,nk_2}+\bar{B}_{66}\sum_{n=1}^{N} C_{k_1n}^{(1)} \bar{\phi}_{yi,nk_2}+\lambda_i \bar{A}_{66}\sum_{m=1}^{M} C_{k_2m}^{(1)} \bar{u}_{i,k_1m}+\lambda_i \bar{B}_{66}\sum_{m=1}^{M} C_{k_2m}^{(1)} \bar{\phi}_{xi,k_1m}=0, \tag{62c}$$

$$\bar{B}_{66}\sum_{n=1}^{N} C_{k_1n}^{(1)} \bar{v}_{i,nk_2}+\bar{D}_{66}\sum_{n=1}^{N} C_{k_1n}^{(1)} \bar{\phi}_{yi,nk_2}+\lambda_i \bar{B}_{66}\sum_{m=1}^{M} C_{k_2m}^{(1)} \bar{u}_{i,k_1m}+\lambda_i \bar{D}_{66}\sum_{m=1}^{M} C_{k_2m}^{(1)} \bar{\phi}_{xi,k_1m}=0, \tag{62d}$$

$$\kappa \bar{A}_{66}\left(\eta_i \bar{\phi}_{yi,k_1k_2}+\lambda_i \sum_{m=1}^{M} C_{k_2m}^{(1)} \bar{w}_{i,k_1m}\right)=0, \tag{62e}$$

at $\xi_i=0,1$, where k_2 is equal to 1 and M when $\xi_i=0$ and $\xi_i=1$, respectively, for CFFF cracked FGM plate.

The compatibility conditions at the crack location are rewritten in dimensionless form as

$$\bar{u}_{1,Nk_2}=\bar{u}_{2,1k_2},\quad \bar{v}_{1,Nk_2}=\bar{v}_{2,1k_2}, \tag{63a}$$

$$\bar{w}_{1,Nk_2}=\bar{w}_{2,1k_2},\ \bar{\phi}_{y1,Nk_2}=\bar{\phi}_{y2,1k_2}, \tag{63b}$$

$$\begin{aligned}\bar{S}_T\left(\phi_{x1,Nk_2}-\phi_{x2,1k_2}\right)&=\bar{B}_{11}\sum_{n=1}^{N} C_{Nn}^{(1)} \bar{u}_{1,nk_2}+\bar{D}_{11}\sum_{n=1}^{N} C_{Nn}^{(1)} \bar{\phi}_{x1,nk_2}\\&+\lambda_1 \bar{B}_{12}\sum_{m=1}^{M} C_{k_2m}^{(1)} \bar{v}_{1,Nm}+\lambda_1 \bar{D}_{12}\sum_{m=1}^{M} C_{k_2m}^{(1)} \bar{\phi}_{y1,Nm},\end{aligned} \tag{63c}$$

$$\begin{aligned}&\bar{A}_{11}\sum_{n=1}^{N} C_{Nn}^{(1)} \bar{u}_{1,nk_2}+\bar{B}_{11}\sum_{n=1}^{N} C_{Nn}^{(1)} \bar{\phi}_{x1,nk_2}+\lambda_1 \bar{A}_{12}\sum_{m=1}^{M} C_{k_2m}^{(1)} \bar{v}_{1,Nm}+\lambda_1 \bar{B}_{12}\sum_{m=1}^{M} C_{k_2m}^{(1)} \bar{\phi}_{y1,Nm}\\&=\frac{\alpha_1}{\alpha_2}\bar{A}_{11}\sum_{n=1}^{N} C_{1n}^{(1)} \bar{u}_{2,nk_2}+\frac{\alpha_1}{\alpha_2}\bar{B}_{11}\sum_{n=1}^{N} C_{1n}^{(1)} \bar{\phi}_{x2,nk_2}+\lambda_1 \bar{A}_{12}\sum_{m=1}^{M} C_{k_2m}^{(1)} \bar{v}_{2,1m}+\lambda_1 \bar{B}_{12}\sum_{m=1}^{M} C_{k_2m}^{(1)} \bar{\phi}_{y2,1m},\end{aligned} \tag{63d}$$

$$\begin{aligned}&\bar{B}_{11}\sum_{n=1}^{N} C_{Nn}^{(1)} \bar{u}_{1,nk_2}+\bar{D}_{11}\sum_{n=1}^{N} C_{Nn}^{(1)} \bar{\phi}_{x1,nk_2}+\lambda_1 \bar{B}_{12}\sum_{m=1}^{M} C_{k_2m}^{(1)} \bar{v}_{1,Nm}+\lambda_1 \bar{D}_{12}\sum_{m=1}^{M} C_{k_2m}^{(1)} \bar{\phi}_{y1,Nm}\\&=\frac{\alpha_1}{\alpha_2}\bar{B}_{11}\sum_{n=1}^{N} C_{1n}^{(1)} \bar{u}_{2,nk_2}+\frac{\alpha_1}{\alpha_2}\bar{D}_{11}\sum_{n=1}^{N} C_{1n}^{(1)} \bar{\phi}_{x2,nk_2}+\lambda_1 \bar{B}_{12}\sum_{m=1}^{M} C_{k_2m}^{(1)} \bar{v}_{2,1m}+\lambda_1 \bar{D}_{12}\sum_{m=1}^{M} C_{k_2m}^{(1)} \bar{\phi}_{y2,1m},\end{aligned} \tag{63e}$$

$$\begin{aligned}&\overline{A}_{66}\sum_{n=1}^{N}C_{Nn}^{(1)}\overline{v}_{1,nk_2}+\overline{B}_{66}\sum_{n=1}^{N}C_{Nn}^{(1)}\overline{\phi}_{y1,nk_2}+\lambda_1\overline{A}_{66}\sum_{m=1}^{M}C_{k_2m}^{(1)}\overline{u}_{1,Nm}+\lambda_1\overline{B}_{66}\sum_{m=1}^{M}C_{k_2m}^{(1)}\overline{\phi}_{x1,Nm}=\\&\frac{\alpha_1}{\alpha_2}\overline{A}_{66}\sum_{n=1}^{N}C_{1n}^{(1)}\overline{v}_{2,nk_2}+\frac{\alpha_1}{\alpha_2}\overline{B}_{66}\sum_{n=1}^{N}C_{1n}^{(1)}\overline{\phi}_{y2,nk_2}+\lambda_1\overline{A}_{66}\sum_{m=1}^{M}C_{k_2m}^{(1)}\overline{u}_{2,1m}+\lambda_1\overline{B}_{66}\sum_{m=1}^{M}C_{k_2m}^{(1)}\overline{\phi}_{x2,1m},\end{aligned}\tag{63f}$$

$$\begin{aligned}&\overline{B}_{66}\sum_{n=1}^{N}C_{Nn}^{(1)}\overline{v}_{1,nk_2}+\overline{D}_{66}\sum_{n=1}^{N}C_{Nn}^{(1)}\overline{\phi}_{y1,nk_2}+\lambda_1\overline{B}_{66}\sum_{m=1}^{M}C_{k_2m}^{(1)}\overline{u}_{1,Nm}+\lambda_1\overline{D}_{66}\sum_{m=1}^{M}C_{k_2m}^{(1)}\overline{\phi}_{x1,Nm}=\\&\frac{\alpha_1}{\alpha_2}\overline{B}_{66}\sum_{n=1}^{N}C_{1n}^{(1)}\overline{v}_{2,nk_2}+\frac{\alpha_1}{\alpha_2}\overline{D}_{66}\sum_{n=1}^{N}C_{1n}^{(1)}\overline{\phi}_{y2,nk_2}+\lambda_1\overline{B}_{66}\sum_{m=1}^{M}C_{k_2m}^{(1)}\overline{u}_{2,1m}+\lambda_1\overline{D}_{66}\sum_{m=1}^{M}C_{k_2m}^{(1)}\overline{\phi}_{x2,1m},\end{aligned}\tag{63g}$$

$$\eta_1\overline{\phi}_{x1,Nk_2}+\sum_{n=1}^{N}C_{Nn}^{(1)}\overline{w}_{1,nk_2}=\eta_1\overline{\phi}_{x2,1k_2}+\frac{\alpha_1}{\alpha_2}\sum_{n=1}^{N}C_{1n}^{(1)}\overline{w}_{2,nk_2}\ .\tag{63h}$$

The unknown quantities in the vector form are written as

$$\mathbf{d}=\left\{\left\{\overline{u}_{i,k_{12}}\right\},\left\{\overline{v}_{i,k_{12}}\right\},\left\{\overline{w}_{i,k_{12}}\right\},\left\{\overline{\phi}_{xi,k_{12}}\right\},\left\{\overline{\phi}_{yi,k_{12}}\right\}\right\}^{\mathrm{T}},\ k_{12}=1,\ 2,\ \mathrm{K},\ N\times M,\tag{64}$$

where

$$k_{12}=N\times\left(k_1-1\right)+k_2,k_1=1,2,\mathrm{K}\ ,N,k_2=1,2,\mathrm{K}\ ,M.$$

Substituting the boundary and compatibility conditions of the discrete dimensionless form into discretized governing equations Eqs. (52)-(56), then, the system of equation is obtained as

$$\mathbf{Kd}=\mathbf{M}\ddot{\mathbf{d}},\tag{65}$$

where $\mathbf{M}$ is mass matrix; $\mathbf{K}$ represents stiffness matrix.

For the vibration analysis, substituting $\mathbf{d}=\mathbf{d}^{*}\mathrm{e}^{\mathrm{i}\Omega\tau}$ into Eq. (65), the eigenvalue equations can be obtained as

$$\mathbf{Kd}^{*}=-\Omega^{2}\mathbf{Md}^{*},\tag{66}$$

from which the dimensionless nature frequencies and mode shapes are obtained. The relationship between the dimensionless and dimensional frequencies is given in Eq. (33d).

5. Crack identification

The continuous wavelet transform (CWT) has a wide application in the structural damage identification, such as beams [24], plates [31] and shells [26]. In our previous work, a new damage index based on CWT was developed to implement in the crack identification of FGM beams [48]. In this paper, this method is further applied for the crack identification of FGM plates. According to the compatibility conditions at the crack section, there is the discontinuity for the rotations. So, the mode shape can be

treated as an input signal.

An input signal $f(g)$ to be transformed into the wavelet transform coefficients $Wf(b,s)$ by using CWT, i.e., [49]

$$Wf(b,s)=f(g)*\tilde{\varphi}_s(b)=\int_{-\infty}^{+\infty}f(g)\tilde{\varphi}_{b,s}\mathrm{d}g, \tag{67}$$

where the star $*$ represents the convolution of two functions; the mother wavelet function $\varphi(g)$ is transformed to a series of wavelet function $\varphi_{b,s}=\frac{1}{\sqrt{s}}\varphi\left(\frac{g-b}{s}\right)$ by the translation parameter b and scale parameter s; and $\tilde{\varphi}(g)$ denotes the complex conjugate of $\varphi(g)$ that satisfies

$$\int_{-\infty}^{+\infty}\frac{\left|\hat{\varphi}(\varpi)\right|^2}{|\varpi|}\mathrm{d}\varpi=C_\varphi<+\infty, \tag{68}$$

where $\hat{\varphi}(\varpi)$ is the Fourier transform of the wavelet function $\varphi(g)$. Eq. (70) implies that $\varphi(g)$ has a zero average,

$$\int_{-\infty}^{+\infty}\varphi(g)\mathrm{d}g=0. \tag{69}$$

For crack identification, the mode shapes of cracked FGM plates are decomposed into wavelet coefficients by CWT along the x- and y-axes, respectively. The wavelet coefficients are defined by

$$Wf_x(b,s)=w(x,y_0)*\tilde{\varphi}_s(b),\qquad Wf_y(b,s)=w(x_0,y)*\tilde{\varphi}_s(b). \tag{70}$$

The wavelet coefficient modulus may show sudden changes at the crack location and boundaries. The large value at the boundaries results in the confusion for crack identification, namely, edge effect [50]. The maximum value of the wavelet coefficient modulus always occurs at the crack location when the scale parameter varies. In certain scale s_0 and spatial position b_0, $Wf(b_0,s_0)$ is referred to be the wavelet coefficient maxima if it satisfies

$$\frac{\partial Wf(b_0,s_0)}{\partial b}=0\ . \tag{71}$$

Utilizing the character about the maxima of wavelet coefficient modulus, the damage index (DI) for crack identification in plate-like structures at (x_0,y_0) can be defined by

$$DI(x_0,y_0)=\sum_{s=s_{\min}}^{s_{\max}}DWf_x+\sum_{s=s_{\min}}^{s_{\max}}DWf_y=DI(x)\big|_{y=y_0}+DI(y)\big|_{x=x_0}, \tag{72}$$

where $s_{\min}$ and $s_{\max}$ are the minimum and maximum scale parameter, respectively;

$$DWf_x = \begin{cases} 0 & , \dfrac{\partial Wf_x(b,s)}{\partial b} \neq 0, \\ 1 & , \dfrac{\partial Wf_x(b,s)}{\partial b} = 0, \end{cases} \quad , \quad DWf_y = \begin{cases} 0 & , \dfrac{\partial Wf_y(b,s)}{\partial b} \neq 0, \\ 1 & , \dfrac{\partial Wf_y(b,s)}{\partial b} = 0, \end{cases} \quad . \tag{73}$$

The vanishing moment of wavelet function have important effect on crack detection [51]. The symlets wavelet with 8 vanishing moment is selected as the mother wavelet function to conduct the crack localization in FGM plates. The peak of DI indicates the existence of crack and its location. Meanwhile, the merit of the present method is that the edge effect is significantly decreased by introducing the DI.

6. Results and discussion

The numerical results of the vibration and crack identification of cracked FGM plates with various boundary conditions are presented in this section. Unless otherwise stated, the parameters of FGM plates are assumed as h = 0.01 m, L_x =0.1 m and L_y =0.1 m. The top and bottom surfaces of FGM plates are fabricated by SUS304 and Si_3N_4, respectively, and their properties are given in Table 1. In the ABAQUS modeling of SIFs, the FGM layer is discretized into 31 sub-layers. The total numbers of the grid points N and M are taken as N=M for simplicity.

6.1 Comparison and convergence study

To validate linear spring model, the mode I SIFs in the isotropic homogeneous layer and FGM layers with the exponential varying properties are calculated to compare with the reported results. The layer slenderness ratio is considered as 10. The thickness and length of the layer are assumed as 24 mm and 240 mm, respectively. Table 3 compares the present normalized SIFs $\bar{K}_{\mathrm{I}}$ for a homogeneous layer with results given by Tada et al. [52]. The Young's modulus and Poisson's ratio of each layer are constant: $E = 20\mathrm{GPa}$ and $\mu = 0.33$. Our results are in good agreement with the results in [52].

For the graded layer with exponentially varying Young's modulus,

$$E(z) = E_0 e^{\beta z}, \tag{82}$$

where $\beta = \ln(E_b / E_t)/h$ and E_0 is the Young's modulus at $z = 0$. Table 4 compares the present SIFs

with results given by Erdogan and Wu [53] and Song et al. [54]. The Young's modulus of the top surface is equal to 20GPa and Poisson's ratio is constant, μ=0.33. Again, a good agreement is achieved.

Table 5 shows the convergence of the dimensionless fundamental frequency ($\frac{L_x}{h}\Omega$) for the intact FGM plates made of SUS304/Si_3N_4. The parameters of the intact FGM plate are taken as L_x=0.1 m, L_y=0.1 m, h = 0.01 m and n = 2. By increasing grid points N, the accuracy of results is improved, and the results are converged to Zhao et al.'s results [55] when N is greater than 13 for all boundary conditions. Hence, N=13 is applied in the later numerical simulation.

Table 6 lists the fundamental frequencies ($\frac{\sqrt{12}L_y^{\,2}}{L_x h}\Omega$) of cracked homogeneous plates with L_x=3m, L_y=2m, a/h=0.5 and h/L_y=0.2. The parameters in this example are used as n=0, μ_t=0.3 and κ=0.86667. The results given by Hosseini-Hashemi et al. [56] are also given for comparison. It shows a good agreement again.

6.2 Vibration analysis

The effect of the graded index n on the relationship of the dimensionless fundamental frequency Ω versus the crack location L_1 / L_x for cracked FGM plates is depicted in Fig. 3 with a/h=0.3. It is found that the frequency Ω reduces when the graded index changes from 0 to 2. The crack location has marked influence on the frequency of FGM plates with different boundary conditions. The frequency curves are symmetric for the FGM plate with symmetric boundary conditions, such as CCCC and HHHH plates. The curves have the turning points at L_1 / L_x = 0.2, 0.5 and 0.8 for the CCCC plate, at L_1 / L_x = 0.2 and 0.6 for the CCHH plate, and at L_1 / L_x = 0.5 for the HHHH plate. The fundamental frequency of the CFFF FGM plate becomes larger as the crack moves from the clamped edge to the free edge.

Fig. 4 shows the effect of the graded index n on the relationship of the fundamental frequency Ω versus the crack depth a/h for cracked FGM plates with L_1/L_x=0.5. It is seen that the frequency is very sensitive to crack depth. The frequency reduces with increasing crack depth. Figs. 5-8 highlight the mode shape of intact and cracked CFFF, HHHH, CCHH, CCCC FGM plates with a/h=0.3, L_1/L_x=0.5 and n=2, respectively. A slight difference between the intact and cracked plates is observed for CFFF, HHHH,

CCHH, CCCC FGM plates.

As observed in Fig. 4, crack strongly affects the frequency of FGM plates. However, it is difficult to use these results for the damage identification of cracked plates. The reason is that the frequency change is difficult to provide the effective information for localizing the crack in FGM plates. Moreover, in Figs. 5-8, the mode shape cannot be employed directly for the damage identification because it is insensitive to the crack. However, the application of the CWT enables the mode shape to provide useful information for the damage identification. The next sub-section will use the novel crack identification method based on the mode shape and CWT as presented in Section 5.

6.3 Damage identification based on CWT

Figs. 9-12 present the wavelet coefficients modulus of cracked FGM plates with s=16, a/h=0.3, L_1/L_x=0.5 and n=2. The deflection data of plates with 501×501 sampling points are analyzed by the sym8 wavelet. For CCCC, CCHH and HHHH FGM plates in Figs. 10a-12a, the wavelet coefficient modulus $|Wf_x|$ has the large amplitude at the crack location (L_1/L_x=0.5) and boundary ends. For the CFFF FGM plate in Fig. 9a, the value of $|Wf_x|$ at the free end is too large to observe the sharp transition at the crack location. Figs. 9b-12b illustrate the wavelet coefficient modulus $|Wf_y|$ only has the large amplitude at boundary ends because the crack is along the x-direction.

Figs. 13-16 show the wavelet coefficient modulus with varying scale parameter s for the cracked FGM plates with a/h=0.3, L_1/L_x=0.5 and n=2. The modes at y=0.5 and x=0.5 are treated as the input signals of the CWT to obtained $|Wf_x|$ and $|Wf_y|$, respectively. As can be seen in Figs. 13(a)-16(a), the wavelet coefficient modulus $|Wf_x|$ is convergent at the crack location and boundary with reducing the scale parameter. For varying scale parameter, the maximum wavelet coefficient modulus always occurs at the crack location. In particular, the observable peak of the wavelet coefficient modulus $|Wf_x|$ does not occur at the crack location for the CFFF plate because of the edge effect. Similarly, the wavelet coefficient modulus $|Wf_y|$ in Figs. 13b-16b does not have clear change at the crack location.

In Figs. 9-16, we can find that the wavelet coefficient modulus based damage identification does not work well because of the edge effect of cracked plates. Therefore, we suggest to use the damage index (DI) in Eq. (72) for the damage identification. Fig. 17 gives the DI of cracked FGM plates with a/h=0.3, L_1/L_x=0.5 and n=2. The range of the scale parameter is taken as 1-32. For all plates, the peak in DI occur at the crack location so that the crack can be localized accurately. Furthermore, the edge effect is reduced for

all types of boundary conditions by using DI. We can see the clear peak at the crack location for the CFFF FGM plate, while it is not observed in the method based on wavelet coefficient modulus.

For the practical measurement, the mode shape may be polluted by the noise. The effect of the noise should be considered in the damage detection method [32]. To simulate the noisy condition, white Gaussian noise is mixed with the normalized mode shape [57]. Fig. 18 shows the DI of the cracked FGM plates with the noisy condition 80 dB. The minimum and maximum scale parameters and the maximum scale parameter are taken as $s_{\min}=1$ and $s_{\max}=64$, respectively. We can see that the proposed method performs well under the measurement noise for CFFF, HHHH, CCHH, CCCC FGM plates.

7. Conclusions

This paper investigates the free vibration and crack identification of FGM plate with a through-width edge crack. The mode shapes of cracked FGM plates are decomposed into wavelet coefficients with CWT along the *x*- and *y*- directions, respectively. Based on maxima of calculated wavelet coefficients modulus in the varying scale, a novel damage index is proposed to conduct the crack localization in cracked FGM plates. The robustness of the damage index is studied under the noise condition. We can conclude that:

1. The crack significantly affects the frequency of the FGM plate, while the mode shape is insensitive to the crack.
2. The crack identification is hardly achievable by using the effect of the crack on frequency and mode shape directly.
3. The wavelet coefficient modulus based damage identification does not work well because of the edge effect of cracked plates.
4. The proposed damage index is able to localize cracks accurately and reduce the edge effect. The crack location is implied by the maximum damage index.
5. The developed method performs well with the measurement noise for the four types of considered boundary conditions.

Acknowledgements

The work presented in the paper is supported by National Natural Science Foundation of China (Grant No. 11725207).

Data Availability Statement

All data, models, or code generated or used during the study are available from the corresponding author by request.

References

[1] Koizumi M. FGM activities in Japan. Compos Part B-Eng 1997; 28: 1–4.

[2] Shen HS. Functionally Graded Materials Nonlinear Analysis of Plates and Shells. CRC Press, Boca Raton, 2009.

[3] Shen HS, Wang ZX. Assessment of Voigt and Mori-Tanaka models for vibration analysis of functionally graded plates. Compos Struct 2012; 94: 2197–2208.

[4] Gayen D, Tiwari R and Chakraborty D. Static and dynamic analyses of cracked functionally graded structural components: A review. Compos Part B-Eng 2019; 173: 106982.

[5] Abbas MR, Uday MB, Noor AM, Ahmad N, Rajoo S. Microstructural evaluation of a slurry based Ni/YSZ thermal barrier coating for automotive turbocharger turbine application. Mater Design 2016; 109: 47-56.

[6] Cho JR and Park HJ. High strength FGM cutting tools: finite element analysis on thermoelastic characteristics. J Mater Process Tech 2002; 130–131: 351-356.

[7] Miyamoto Y, Kaysser WA, Rabin BH, Kawasaki A, Ford RG. Functionally graded materials: design, processing and application. London: Kluwer Academic Publishers, 1999.

[8] Naebe M and Shirvanimoghaddam K. Functionally graded materials: A review of fabrication and properties. Appl Mater Today 2016; 5: 223–245.

[9] Xu F, Zhang X and Zhang H. A review on functionally graded structures and materials for energy absorption. Eng Struct 2018; 171: 309–325.

[10] Sha G, Radzieński M, Cao M, Ostachowicz W. A novel method for single and multiple damage detection in beams using relative natural frequency changes. Mech Syst Signal Pr 2019; 132: 335–352.

[11] Pan J, Zhang Z, Wu J, Ramakrishnan KR, Singh HK. A novel method of vibration modes selection for improving accuracy of frequency-based damage detection. Compos Part B-Eng 2019; 159: 437–446.

[12] Fan W and Qiao P. Vibration-based damage identification methods: a review and comparative study. Struct Health Monit 2011; 10: 83-111.

[13] Gomes GF, Mendez YAD, Alexandrino PDL, da Cunha SS, Ancelotti AC. A Review of Vibration Based Inverse Methods for Damage Detection and Identification in Mechanical Structures Using Optimization Algorithms and ANN. Arch Comput Method E 2019; 26:883–897.

[14] Baqersad J, Poozesh P, Niezrecki C, Avitabile, P. Photogrammetry and optical methods in structural dynamics – A review. Mech Syst Signal Pr 2017; 86: 17-34.

[15] Reu PL, Rohe DP and Jacobs LD. Comparison of DIC and LDV for practical vibration and modal measurements. Mech Syst Signal Pr 2017; 86: 2–16.

[16] Chen DM, Xu YF and Zhu WD. Non-model-based multiple damage identification of beams by a continuously scanning laser Doppler vibrometer system. Measurement 2018; 115: 185-196.

[17] Pandey AK, Biswas M and Samman MM. Damage detection from changes in curvature mode shapes. J Sound Vib 1991; 145:321-332.

[18] dos Santos JVA, Lopes HMR, Vaz M, Soares CMM, Soares CAM, de Freitas MJM. Damage localization in laminated composite plates using mode shapes measured by pulsed TV holography. Compos Struct 2006; 76: 272–281.

[19] Xu W, Cao MS, Ostachowicz W, Radzienski, M, Xia N. Two-dimensional curvature mode shape method based on wavelets and Teager energy for damage detection in plates. J Sound Vib 2015; 347: 266-278.

[20] Qiao P, Lu K, Lestari W, Wang JL. Curvature mode shape-based damage detection in composite laminated plates. Compos Struct 2007; 80: 409–428.

[21] Dessi D and Camerlengo G. Damage identification techniques via modal curvature analysis: Overview and comparison. Mech Syst Signal Pr 2015; 52-53: 181–205.

[22] Yan YJ, Cheng L, Wu ZY, Yam LH. Development in vibration-based structural damage detection technique. Mech Syst Signal Pr 2007; 21: 2198–2211.

[23] Rucka M and Wilde K. Crack identification using wavelets on experimental static deflection profiles. Eng Struct 2006; 28: 279-288.

[24] Sha GG, Radzienski M, Soman R, Cao MS, Ostachowicz W, Xu W. Multiple damage detection in laminated composite beams by data fusion of Teager energy operator-wavelet transform mode shapes. Compos Struct 2020; 235: 111798.

[25] Zhu XQ and Law SS. Wavelet-based crack identification of bridge beam from operational deflection time history. Int J Solids Struct 2006; 43: 2299-2317.

[26] Parrany AM. Damage detection in circular cylindrical shells using active thermography and 2-D discrete wavelet analysis. Thin Wall Struct 2019; 136: 34–49.

[27] Mallat S and Hwang WL. Singularity detection and processing with wavelets. IEEE T Inform Theory 1992; 38: 617-643.

[28] Douka E, Loutridis S and Trochidis A. Crack identification in plates using wavelet analysis. J Sound Vib 2004; 270: 279–295.

[29] Fan W and Qiao P. A 2-D continuous wavelet transform of mode shape data for damage detection of plate structures. Int J Solids Struct 2009; 46: 4379–4395.

[30] Katunin A. Damage identification in composite plates using two-dimensional B-spline wavelets. Mech Syst Signal Pr 2011; 25: 3153–3167.

[31] Zhou J and Li Z. Damage detection based on vibration for composite sandwich panels with truss core. Compos Struct 2019; 229: 111376.

[32] Xu W, Ding KQ, Liu JQ, Cao MS, Radzienski M, Ostachowicz W. Non-uniform crack identification in plate-like structures using wavelet 2D modal curvature under noisy conditions. Mech Syst Signal Pr 2019; 126: 469–489.

[33] Khiem NT and Huyen NN. A method for crack identification in functionally graded Timoshenko beam. Nondestruct Test Eva 2017; 32: 319-341.

[34] Yu Z and Chu F. Identification of crack in functionally graded material beams using the p-version of finite element method. J Sound Vib 2009; 325: 69-84.

[35] Yang DL, Hu ZM, Kang CY, Liang J. Damage detection of functionally graded Euler-Bernoulli beam based on element modal strain energy equivalence index. Sci Adv Mater 2018; 10: 1036–1044.

[36] Lu ZR, Lin XX, Chen YM, Huang M. Hybrid sensitivity matrix for damage identification in axially functionally graded beams. Appl Math Model 2017; 41:604-617.

[37] Joshi PV, Gupta A, Jain NK, Salhotra R, Rawani AM, Ramtekkar GD. Effect of thermal environment on free vibration and buckling of partially cracked isotropic and FGM micro plates based on a nonclassical Kirchhoff's plate theory: An analytical approach. Int J Mech Sci 2017; 131–132: 155–170.

[38] Huang CS, McGee OG and Chang MJ. Vibrations of cracked rectangular FGM thick plates. Compos Struct 2011; 93: 1747–1764.

[39] Fantuzzi N, Tornabene F and Viola E. Four-parameter functionally graded cracked plates of arbitrary shape: a GDQFEM solution for free vibrations. Mech Adv Mater Struct 2016; 23: 89-107.

[40] Li DH, Yang X, Qian RL, Xu D. Static and dynamic response analysis of functionally graded material plates with damage. Mech Adv Mater Struct 2020; 27: 94-107.

[41] Wang Y and Wang ZM. Transverse vibration of viscoelastic rectangular plate with linearly varying thickness and multiple cracks. J Sound Vib 2008; 318: 1005–1023.

[42] Yang J, Hao YX, Zhang W, Kitipornchai S. Nonlinear dynamic response of a functionally graded plate with a through-width surface crack. Nonlinear Dynam 2010; 59: 207–219.

[43] Broek D. Elementary Engineering Fracture Mechanics. Dordrecht: Martinus Nijhoff Publishers, 1986.

[44] Ramirez F, Heyliger PR, Pan E. Static analysis of functionally graded elastic anisotropic plates using a discrete layer approach. Compos Part B-Eng 2006; 37: 10–20.

[45] Ke LL, Yang J, Kitipornchai S, Xiang Y. Flexural vibration and elastic buckling of a cracked Timoshenko beam made of functionally graded materials. Mech Adv Mater Struct 2009; 16: 488-502.

[46] Efraim E, Eisenberger M. Exact vibration analysis of variable thickness thick annular isotropic and FGM plates. Compos Struct 2007; 299: 720–738.

[47] Shu C. Differential Quadrature and Its Application in Engineering. London: Springer, 2000.

[48] Zhu LF, Ke LL, Zhu XQ, Xiang Y, Wang YS. Crack identification of functionally graded beams using continuous wavelet transform. Compos Struct 2019; 210: 473–485.

[49] Mallat S. A wavelet tour of signal processing (Second Edition), San Diego: Academic Press, 1999.

[50] Kijewski T and Ksreem A. On the presence of end effects and their melioration in wavelet-based analysis. J Sound Vib 2002; 256: 980-988.

[51] Douka E, Loutridis S and Trochidis A. Crack identification in beams using wavelet analysis. Int J Solids Struct 2003; 40: 3557-3569.

[52] Tada H, Paris PC and Irwin GR. The stress analysis of cracks handbook, third edition. New York: ASME Press, 2000.

[53] Erdogan F and Wu BH. The surface crack problem for a plate with functionally graded properties. J Appl Mech-T ASME 1997; 64:449-456.

[54] Song M, Gong Y, Yang J, Kitipornchai S, Xiang Y. Free vibration and buckling analyses of edge-cracked functionally graded multilayer graphene nanoplatelet-reinforced composite beams resting on an elastic foundation. J Sound Vib 2019; 458: 89-108.

[55] Zhao X, Lee YY and Liew KM. Free vibration analysis of functionally graded plates using the element-free *kp*-Ritz method. J Sound Vib 2009; 319: 918–939.

[56] Hosseini-Hashemi S, Gh HR and Rokni DTH. Exact free vibration study of rectangular Mindlin plates with all-over part-through open cracks. Comput Struct 2010; 88: 1015–1032.

[57] Yang ZB, Radzienski M and Kudela P. Two-dimensional Chebyshev pseudo spectral modal curvature and its application in damage detection for composite plates. Compos Struct 2017; 168: 372–383.

Figure captions

Fig. 1. A cracked FGM plate (a) and the massless rotational spring model (b).

Fig. 2. Multilayer model of cracked FGM strip.

Fig. 3. The effect of graded index n on relation of the fundamental frequency versus the crack location with a/h=0.3: (a) CFFF, (b) CCCC, (c) CCHH, (d) HHHH.

Fig. 4. The effect of graded index n on relation of the fundamental frequency versus the crack depth with L_1/L_x=0.5: (a) CFFF, (b) CCCC, (c) CCHH, (d) HHHH.

Fig. 5. The mode shape of CFFF FGM plates with a/h=0.3, L_1/L_x=0.5 and n=2: (a) intact plate and (b) cracked plate.

Fig. 6. The mode shape of CCCC FGM plates with a/h=0.3, L_1/L_x=0.5 and n=2: (a) intact plate and (b) cracked plate.

Fig. 7. The mode shape of CCHH FGM plates with a/h=0.3, L_1/L_x=0.5 and n=2: (a) intact plate and (b) cracked plate.

Fig. 8. The mode shape of HHHH FGM plates with a/h=0.3, L_1/L_x=0.5 and n=2: (a) intact plate and (b) cracked plate.

Fig. 9. Wavelet coefficient modulus of CFFFF cracked FGM plates with s=16, a/h=0.3, L_1/L_x=0.5 and n=2: (a) $|Wf_x|$ and (b)$|Wf_y|$.

Fig. 10. Wavelet coefficient modulus of CCCC cracked FGM plates with s=16, a/h=0.3, L_1/L_x=0.5 and n=2: (a) $|Wf_x|$ and (b)$|Wf_y|$.

Fig. 11. Wavelet coefficient modulus of CCHH cracked FGM plates with s=16, a/h=0.3, L_1/L_x=0.5 and n=2: (a) $|Wf_x|$ and (b)$|Wf_y|$.

Fig. 12. Wavelet coefficient modulus of HHHH cracked FGM plates with s=16, a/h=0.3, L_1/L_x=0.5 and n=2: (a) $|Wf_x|$ and (b)$|Wf_y|$.

Fig. 13. Wavelet coefficient modulus of deflection lines of the CFFF cracked FGM plate in the scale space (s=1-32) with a/h=0.3, L_1/L_x=0.5 and n=2: (a)$|Wf_x|$ at y=0.5 and (b)$|Wf_y|$ at x=0.5.

Fig. 14. Wavelet coefficient modulus of deflection lines of the CCCC cracked FGM plate in the scale space (s=1-32) with a/h=0.3, L_1/L_x=0.5 and n=2: (a)$|Wf_x|$ at y=0.5 and (b)$|Wf_y|$ at x=0.5.

Fig. 15. Wavelet coefficient modulus of deflection lines of the CCHH cracked FGM plate in the scale space (s=1-32) with a/h=0.3, L_1/L_x=0.5 and n=2: (a)$|Wf_x|$ at y=0.5 and (b)$|Wf_y|$ at x=0.5.

Fig. 16. Wavelet coefficient modulus of deflection lines of the HHHH cracked FGM plate in the scale space (s=1-32) with a/h=0.3, L_1/L_x=0.5 and n=2: (a)$|Wf_x|$ at y=0.5 and (b)$|Wf_y|$ at x=0.5.

Fig. 17. Damage index of cracked FGM plates with a/h=0.3, L_1/L_x=0.5 and n=2: (a) CFFF, (b) CCCC, (c) CCHH, and(d)HHHH.

Fig. 18. Damage index of cracked FGM plates under 80 dB noise condition with a/h=0.3, L_1/L_x=0.5 and n=2: (a)CFFF, (b)CCCC, (c)CCHH, and (d)HHHH.

Table 1 Material property of the components

Material	Young's modulus (GPa)	Mass density (kg / m^3)	Poisson's ratio
SUS304	207.78	8166	0.3177
Si_3N_4	322.27	2370	0.24

Table 2 Normalized SIFs of an FGM ($SUS304/Si_3N_4$) layer with power law distribution

	n			
a / *h*	0	0.5	1	2
0.1	1.0474	0.9239	0.9141	0.9406
0.2	1.0556	0.9649	0.9404	0.9461
0.3	1.1244	1.0534	1.0207	1.0104
0.4	1.2610	1.1989	1.1666	1.1424
0.5	1.4976	1.4413	1.4055	1.3685
0.6	1.9145	1.8628	1.8217	1.7729
0.7	2.7257	2.6726	2.6292	2.5645

Table 3 Normalized SIFs of a homogeneous layer containing an edge crack

a / h	Present	Tada et al. [52]
0.1	1.0474	1.0384
0.2	1.0556	1.0405
0.3	1.1244	1.1080
0.4	1.2610	1.2488
0.5	1.4976	1.4909
0.6	1.9145	1.9215
0.7	2.7257	2.7569

Table 4 Normalized SIFs of an FGM layer with exponential distribution

a/h	$E_2/E_1=0.2$			$E_2/E_1=5$		
	Present	Erdogan and Wu [53]	Song et al. [54]	Present	Erdogan and Wu [53]	Song et al. [54]
0.1	1.6641	1.6743	1.6823	0.6411	0.6385	0.6469
0.2	1.5861	1.5952	1.5978	0.6887	0.6871	0.6973
0.3	1.6011	1.6122	1.6084	0.7791	0.7778	0.7923
0.4	1.7043	1.7210	1.7082	0.9252	0.9236	0.9450
0.5	1.9236	1.9534	1.9246	1.1605	1.1518	1.1901
0.6	2.3385	2.4037	--	1.5636	1.5597	--
0.7	3.1669	3.3536	--	2.3445	2.3360	--

Table 5 Convergence and comparison studies of the fundamental frequency of the intact FGM plates.

N	HHHH	CCCC	CFFF	CCHH
4	5.1183	8.8933	0.4321	7.0740
6	3.0389	5.1971	0.5464	4.0290
8	3.0461	5.1870	0.5469	4.0321
10	3.0460	5.1861	0.5459	4.0312
12	3.0460	5.1859	0.5454	4.0311
13	3.0460	5.1859	0.5453	4.0311
14	3.0460	5.1859	0.5453	4.0311
Zhao et al. [55]	3.0813	5.2874	0.5576	--

Table 6 Comparison of the fundamental frequencies for homogenous edge-cracked plates.

	HHHH		CHCH	
L_1 / L_x	Present	Hosseini-Hashemi et al. [56]	Present	Hosseini-Hashemi et al. [56]
0.25	12.6349	12.5747	14.8453	14.7806
0.5	12.3521	12.4089	14.0615	14.2545

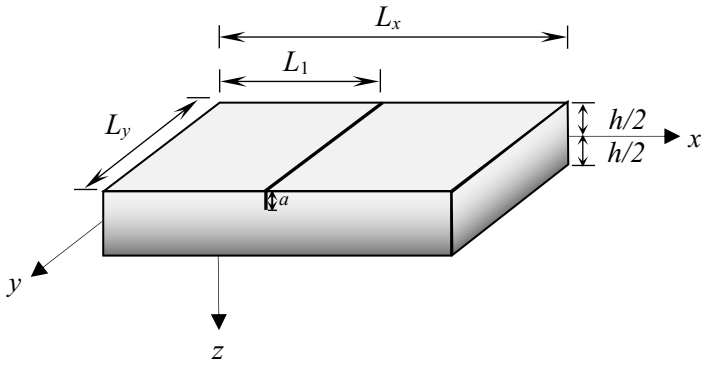

(a)

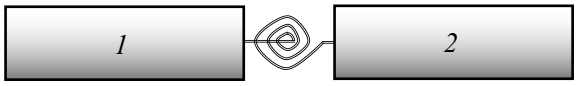

K_T

(b)

Fig. 1. A cracked FGM plate (a) and the massless rotational spring model (b).

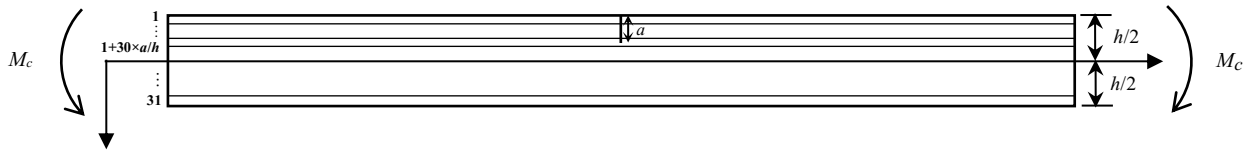

Fig. 2. Multilayer model of cracked FGM strip.

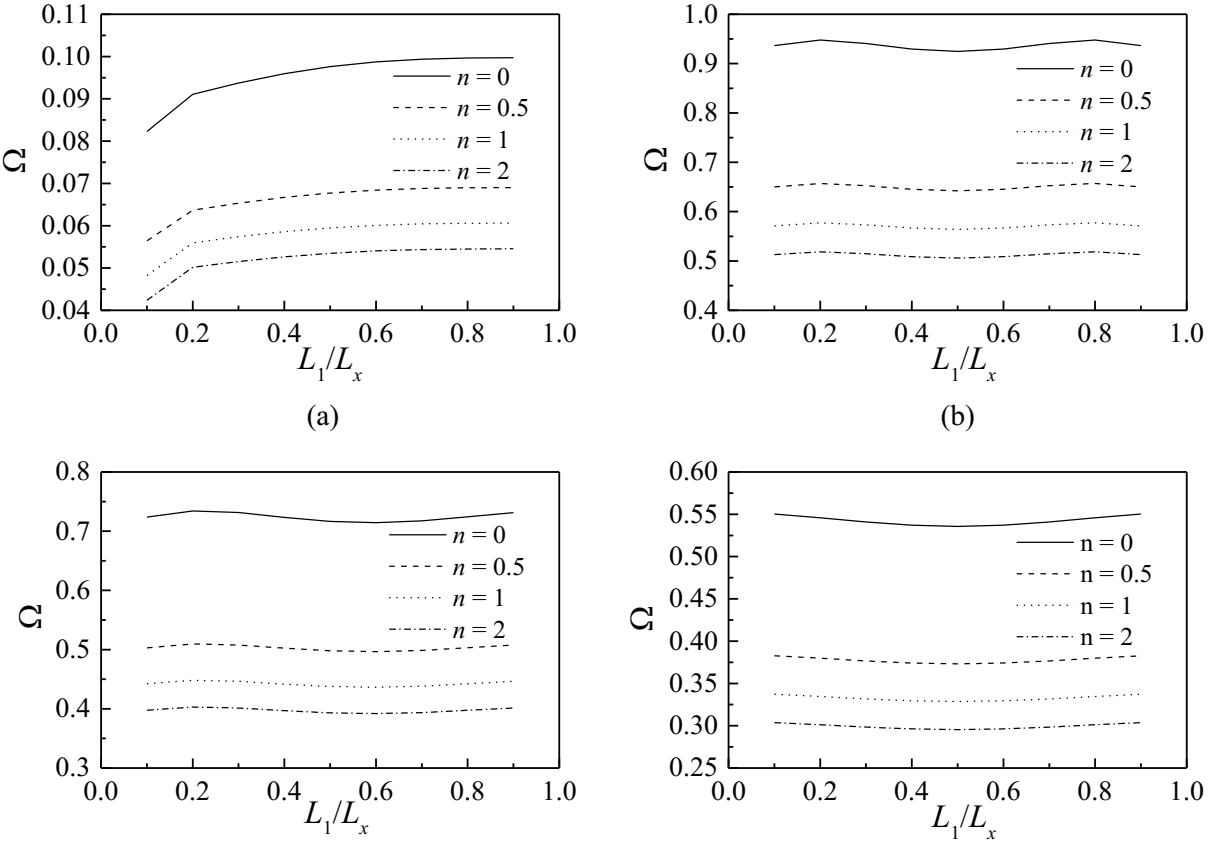

Fig. 3. The effect of graded index *n* on relation of the fundamental frequency versus the crack location with *a*/*h*=0.3: (a) CFFF, (b) CCCC, (c) CCHH, (d) HHHH.

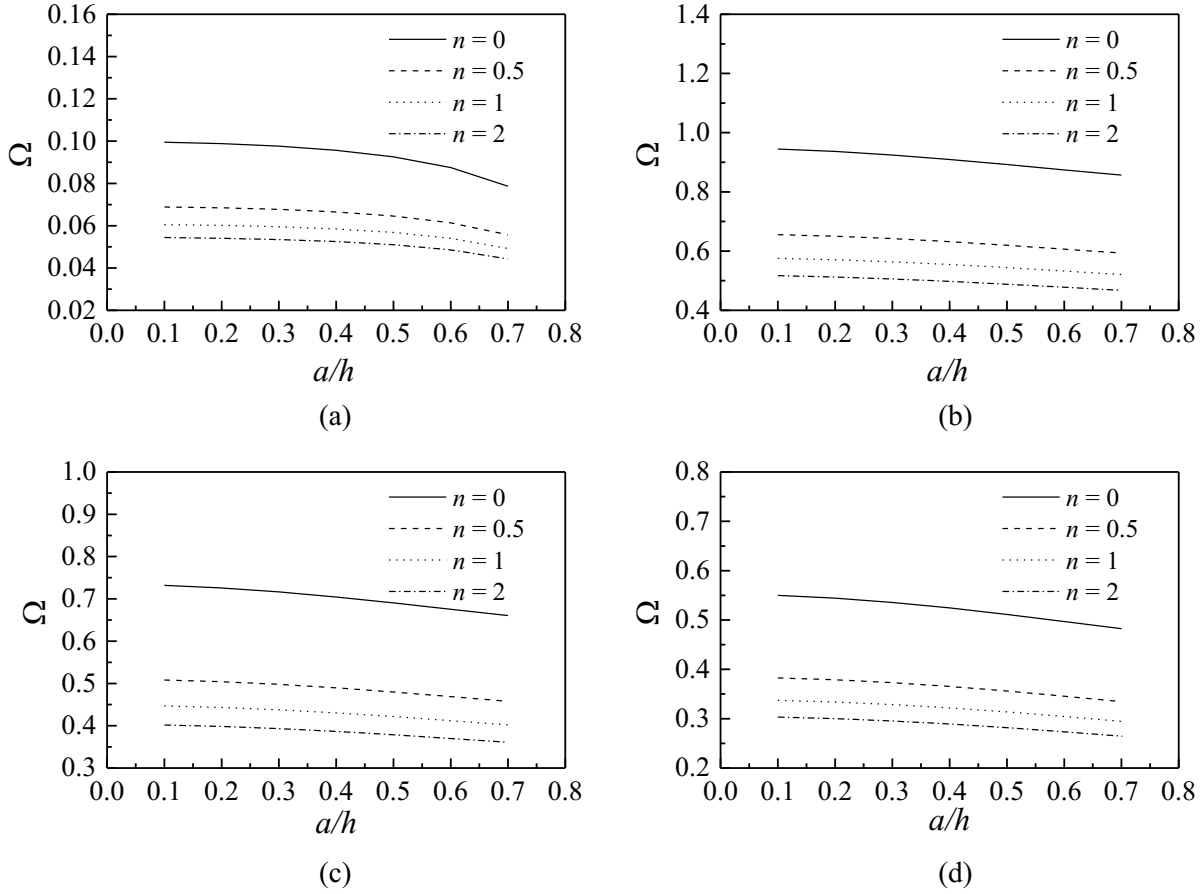

Fig. 4. The effect of graded index n on relation of the fundamental frequency versus the crack depth with L_1/L_x=0.5: (a) CFFF, (b) CCCC, (c) CCHH, (d) HHHH.

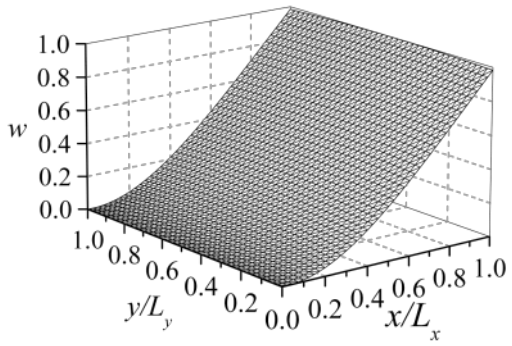

(a)

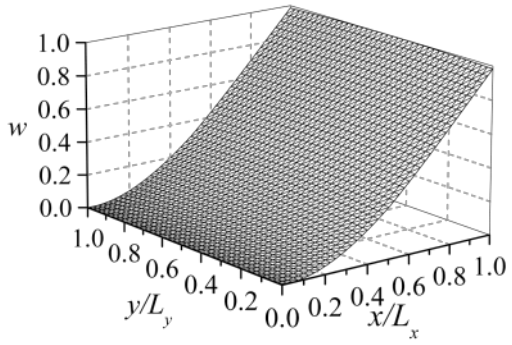

(b)

Fig. 5. The mode shape of CFFF FGM plates with a/h=0.3, L_1/L_x=0.5 and n=2: (a) intact plate and (b) cracked plate.

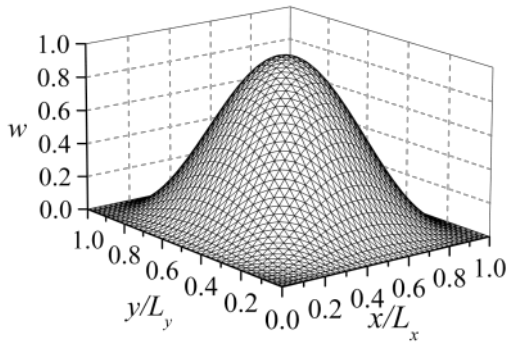

(a)

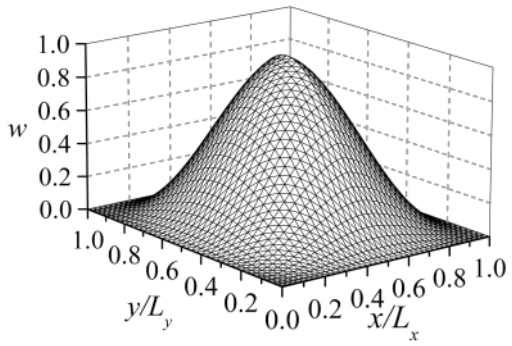

(b)

Fig. 6. The mode shape of CCCC FGM plates with a/h=0.3, L_1/L_x=0.5 and n=2: (a) intact plate and (b) cracked plate.

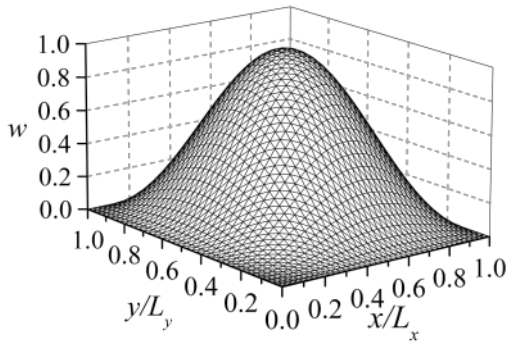

(a)

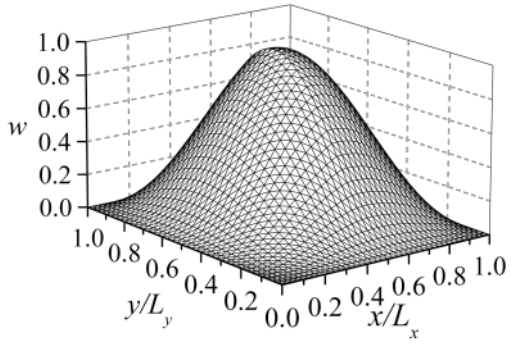

(b)

Fig. 7. The mode shape of CCHH FGM plates with a/h=0.3, L_1/L_x=0.5 and n=2: (a) intact plate and (b) cracked plate.

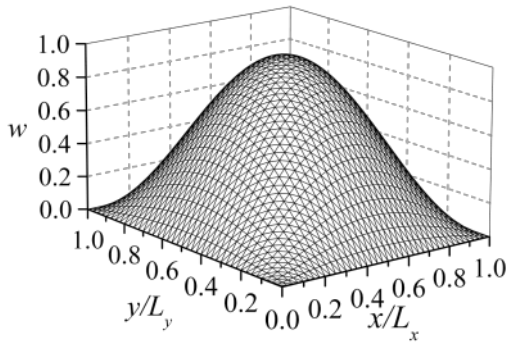

(a)

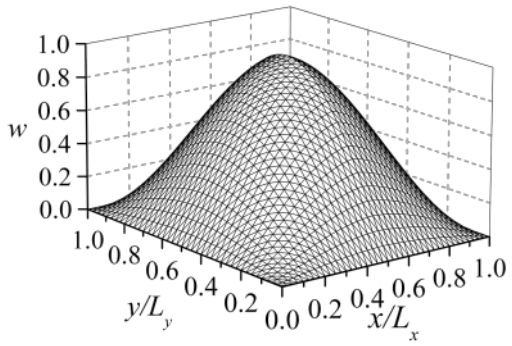

(b)

Fig. 8. The mode shape of HHHH FGM plates with a/h=0.3, L_1/L_x=0.5 and n=2: (a) intact plate and (b) cracked plate.

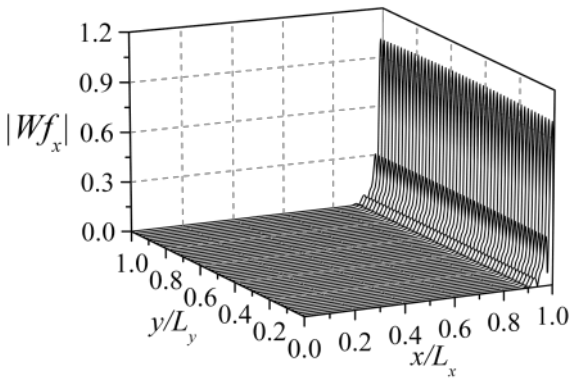

(a)

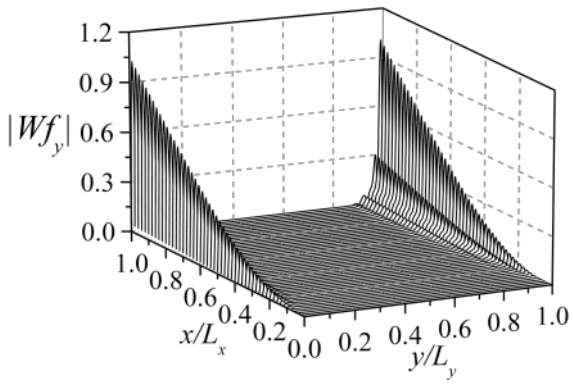

(b)

Fig. 9. Wavelet coefficient modulus of CFFFF cracked FGM plates with s=16, a/h=0.3, L_1/L_x=0.5 and n=2: (a) $|Wf_x|$ and (b) $|Wf_y|$.

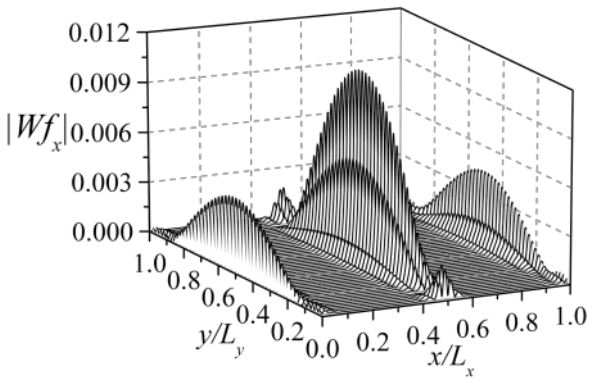

(a)

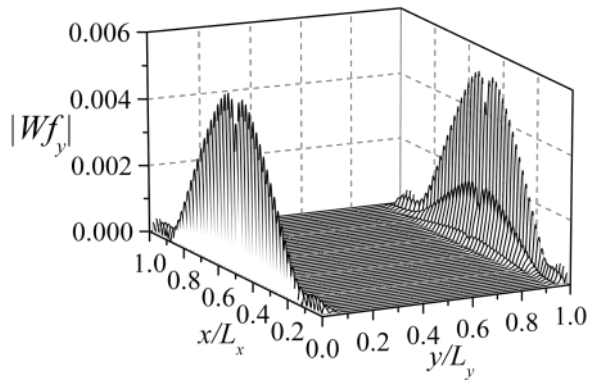

(b)

Fig. 10. Wavelet coefficient modulus of CCCC cracked FGM plates with s=16, a/h=0.3, L_1/L_x=0.5 and n=2: (a) $|Wf_x|$ and (b) $|Wf_y|$.

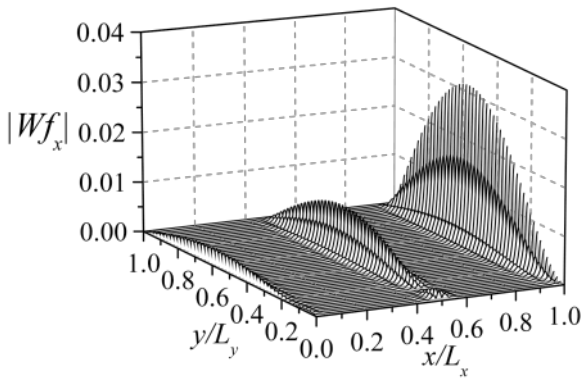

(a)

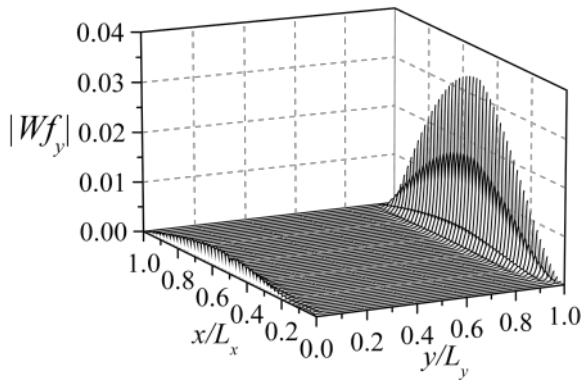

(b)

Fig. 11. Wavelet coefficient modulus of CCHH cracked FGM plates with s=16, a/h=0.3, L_1/L_x=0.5 and n=2: (a) $|Wf_x|$ and (b) $|Wf_y|$.

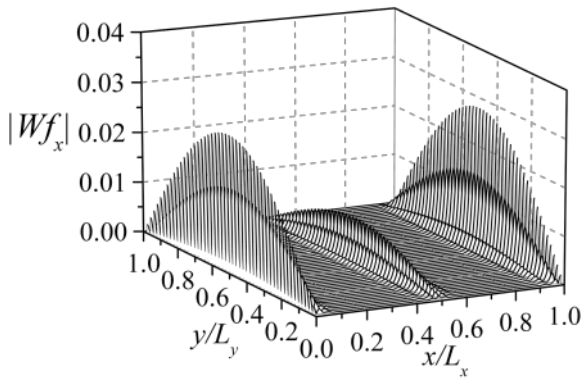

(a)

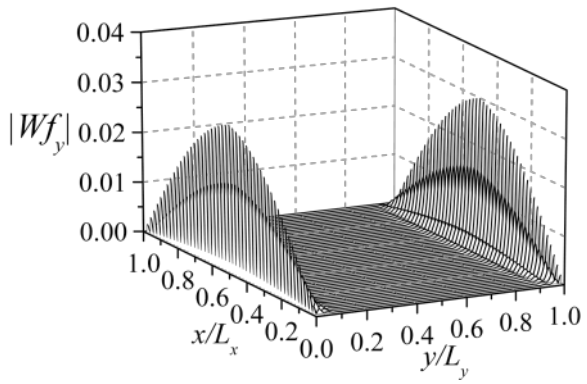

(b)

Fig. 12. Wavelet coefficient modulus of HHHH cracked FGM plates with s=16, a/h=0.3, L_1/L_x=0.5 and n=2: (a) $|Wf_x|$ and (b) $|Wf_y|$.

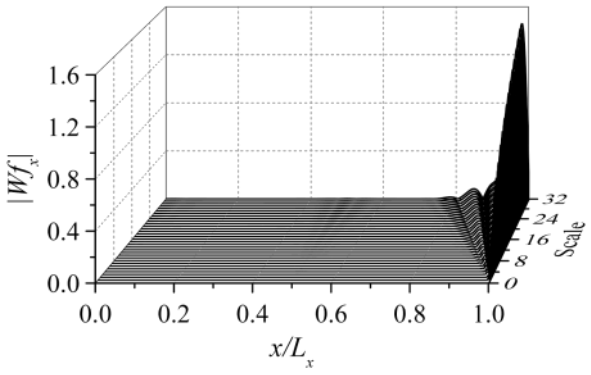

(a)

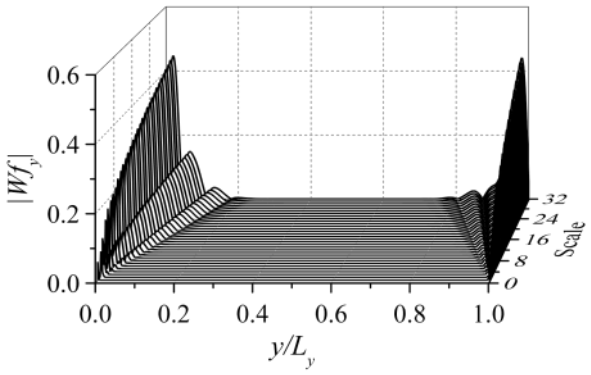

(b)

Fig. 13. Wavelet coefficient modulus of deflection lines of the CFFF cracked FGM plate in the scale space (s=1-32) with a/h=0.3, L_1/L_x=0.5 and n=2: (a) $|Wf_x|$ at y=0.5 and (b) $|Wf_y|$ at x=0.5.

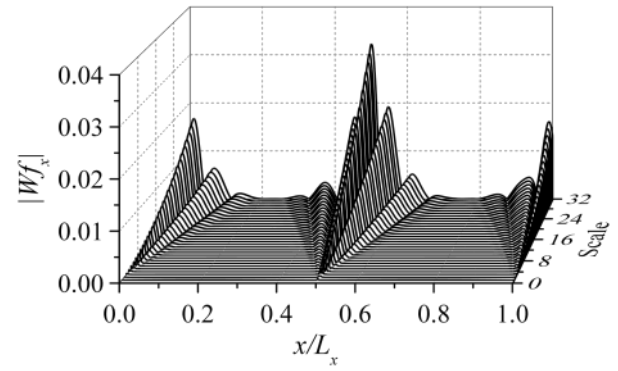

(a)

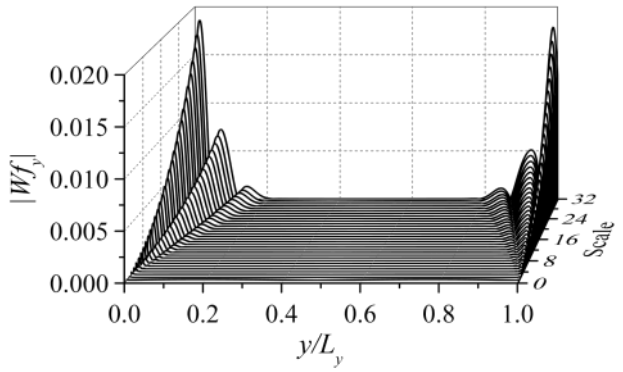

(b)

Fig. 14. Wavelet coefficient modulus of deflection lines of the CCCC cracked FGM plate in the scale space (s=1-32) with a/h=0.3, L_1/L_x=0.5 and n=2: (a) $|Wf_x|$ at y=0.5 and (b) $|Wf_y|$ at x=0.5.

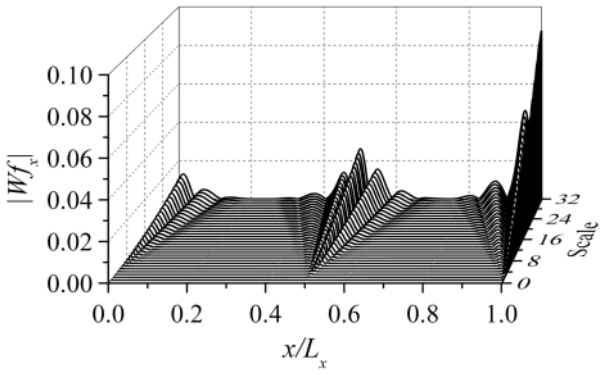

(a)

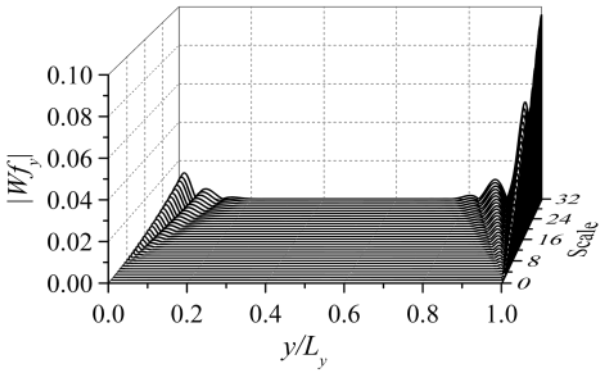

(b)

Fig. 15. Wavelet coefficient modulus of deflection lines of the CCHH cracked FGM plate in the scale space (s=1-32) with a/h=0.3, L_1/L_x=0.5 and n=2: (a) $|Wf_x|$ at y=0.5 and (b) $|Wf_y|$ at x=0.5.

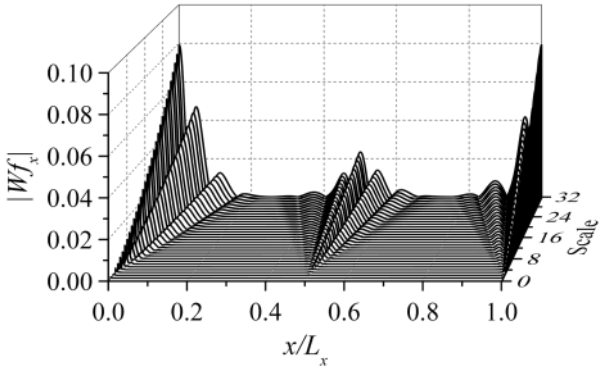

(a)

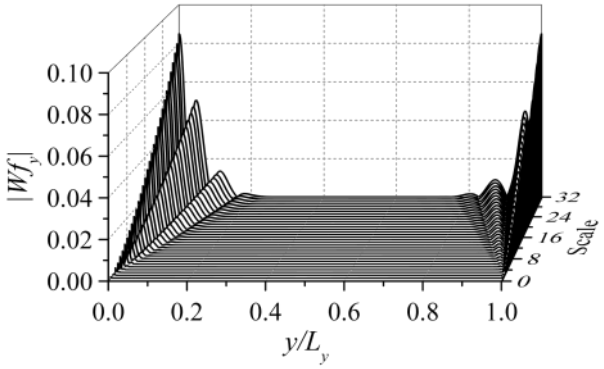

(b)

Fig. 16. Wavelet coefficient modulus of deflection lines of the HHHH cracked FGM plate in the scale space (s=1-32) with a/h=0.3, L_1/L_x=0.5 and n=2: (a) $|Wf_x|$ at y=0.5 and (b) $|Wf_y|$ at x=0.5.

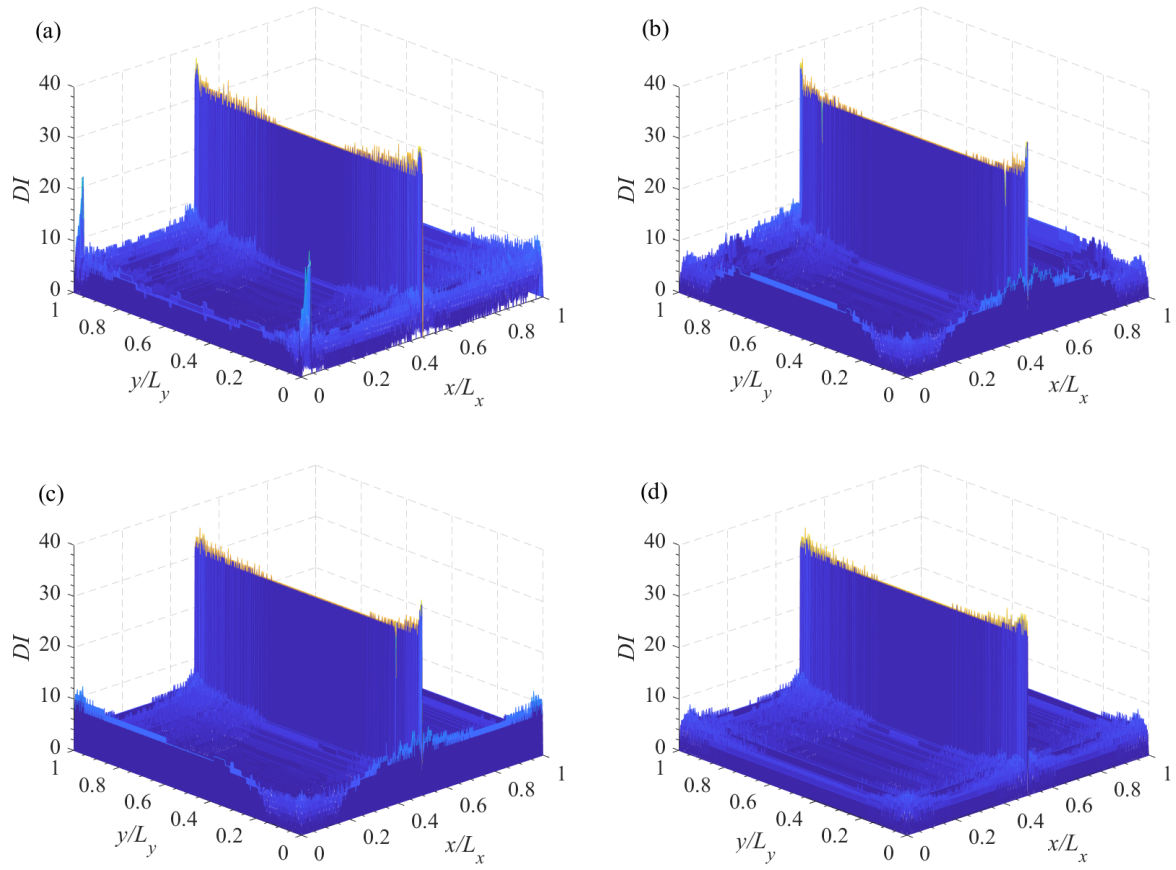

Fig. 17. Damage index of cracked FGM plates with a/h=0.3, L_1/L_x=0.5 and n=2: (a) CFFF, (b) CCCC, (c) CCHH, and (d) HHHH.

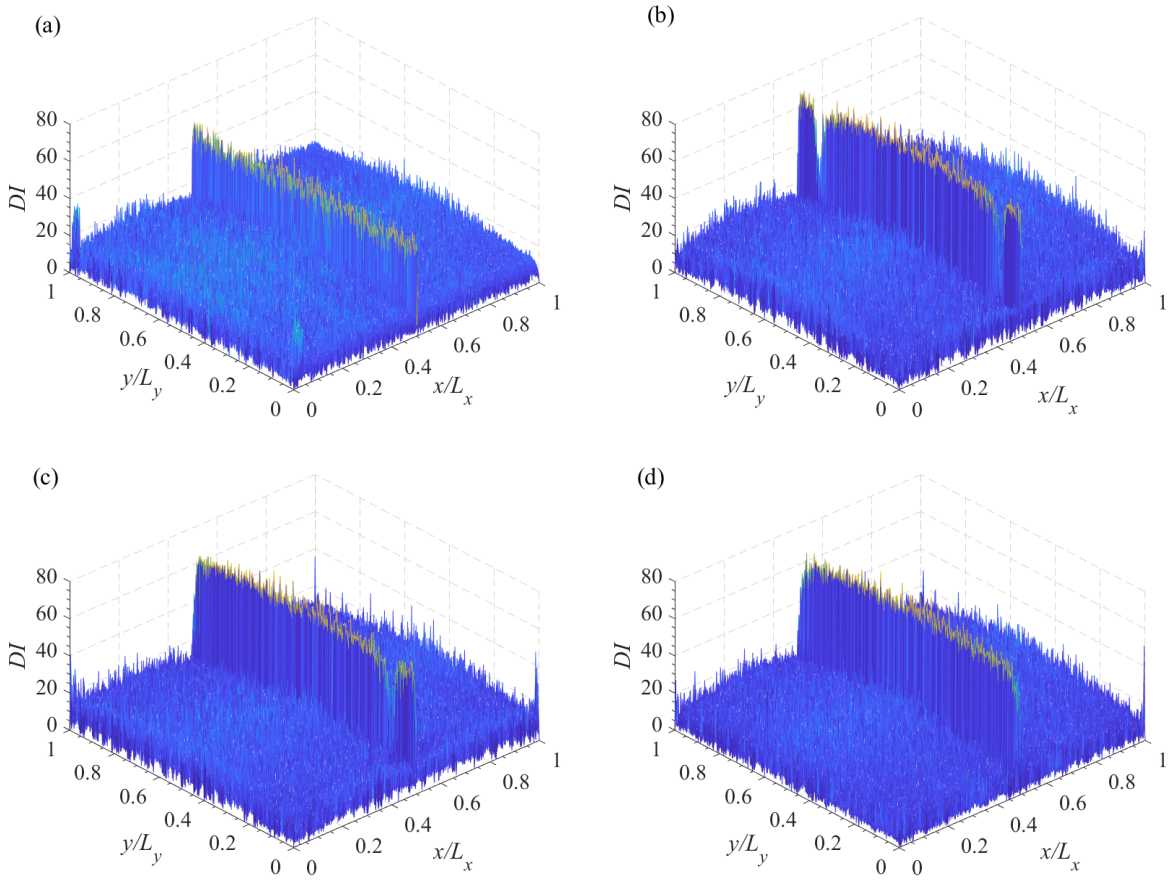

Fig. 18. Damage index of cracked FGM plates under 80 dB noise condition with a/h=0.3, L_1/L_x=0.5 and n=2: (a) CFFF, (b) CCCC, (c) CCHH, and (d) HHHH.